Food Hydrocolloids 137 (2023) 108412

Contents lists available at ScienceDirect

Food Hydrocolloids

journal homepage: www.elsevier.com/locate/foodhyd

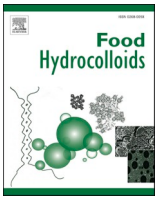

Production of nanoparticles from resistant starch via a simple three-step physical treatment

Eftychios Apostolidis [a,b], Anastasios Stergiou [c], Dimitrios Kioupis [d], Amin Sadeghpour [b], Paraskevi Paximada [b], Glikeria Kakali [d], Ioanna Mandala [a,*]

[a] Agricultural University of Athens, Dept. Food Science & Human Nutrition, Laboratory of Food Process Engineering, Iera Odos 75, 11855, Votanikos, Athens, Greece
[b] School of Food Science and Nutrition, University of Leeds, Leeds, LS2 9JT, UK
[c] Theoretical and Physical Chemistry Institute, National Hellenic Research Foundation, 48 Vassileos Constantinou Avenue, 11635, Athens, Greece
[d] National Technical University of Athens, School of Chemical Engineering, Laboratory of Inorganic and Analytical Chemistry, 9 Heroon Polytechniou St, 15773, Athens, Greece

ARTICLE INFO

Keywords:
Physical modification
Resistant starch type 2
Starch nano-particles
Morphology

ABSTRACT

The purpose of this study was to physically process Hi-maize 260® granules and investigate the size reduction towards obtaining starch nano-particles, stable in aqueous suspensions. We developed a novel sequential three-step physical process consisting of hydrothermal gelatinization, nano-precipitation and ultrasonic treatment. Ultrasonication proved to be a key-step to dismantle the ununiform agglomerates nanoparticles produced by the nanoprecipitation of the hydrothermally gelatinized starch, furnishing uniform nanoparticles (170 nm). This was unveiled by complementary Dynamic Light Scattering (DLS) and electrophoretic mobility (Z-potential) studies, as well as fluorescence spectroscopy. Notably, this 3-step process reduced the size of the starch particles to nano dimensions without destroying their crystallographic structure, as shown by X-ray diffraction (XRD) and Small Angle X-ray Scattering (SAXS), or changing. their chemical integrity, as validated by Fourier transform infrared spectroscopy (FTIR) and Thermogravimetric Analysis (TGA) analyses. Finally, we evaluated the hydrophobicity of the isolated nanoparticles by employing the sessile drop method, witnessing an increment to the hydrophobicity as a result of size reduction. Collectively, we developed a handy protocol enroot to reduce the size of RS2 starch particles enabling its application in an array of meaningful real-world food applications.

1. Introduction

Starch is one of the most abundant storage polysaccharides in plant seed amyloplasts. It is a type of natural carbohydrate mainly composed of variable ratios of two distinct glycose molecules, amylose and amylopectin (Junejo et al., 2022). Structurally, starch is a homo-polysacharide that contains amylose (AM), a D-glucosyl linear polymer chain connected by a-(1,4)-glycosidic linkage and amylopectin (AP), a highly branched polymer with a-(1,4)-glucosidic linkages in the glucan chain and a-(1,6)-glucosidic bonds at the branch points after every 20 to 30 glucose units (Vamadevan & Bertoft, 2015). The molecular structure is based on these components on different ratios (~70%/30%, AP/AM for native starch) that occur in the form of discrete, semi-crystalline aggregate forms named starch granules (Lawal, 2019; Zhong et al., 2020). Starch granules exhibit an "onion-like" structure with semi-crystalline growth rings, of alternating amorphous and crystalline lamellae while the cluster arrangement of amylopectin side chains is responsible for the crystallinity (Angellier et al., 2005; Bertoft, 2017; Copeland et al., 2009; Hernandez-Hernandez et al., 2022).

Concerning its nutritional aspect, starch is divided into three categories based on the hydrolysis rate: rapidly digested starch (RDS), slowly digested starch (SDS), and resistant starch (RS) (Englyst et al., 1982, 1992). Among them, RS is a valuable ingredient to the food industry that exhibits various benefits for metabolic health, whereas its importance is further substantiated by the fact that the RS type holds a health claim from the EFSA. The digestion of starch is influenced by many parameters, including the amylose:amylopectin ratio, its granular architecture, shape, size, molecular composition, and crystalline structure. These structural patterns significantly affect its thermal, digestive and soluble properties in water at room temperature, leading to functional limitations in its application in the food industry (Benmoussa et al., 2007; Chung et al., 2011; L. J. Zhu et al., 2011). Efforts are geared towards

* Corresponding author.
E-mail address: imandala@aua.gr (I. Mandala).

https://doi.org/10.1016/j.foodhyd.2022.108412
Received 11 September 2022; Received in revised form 7 December 2022; Accepted 12 December 2022
Available online 17 December 2022

adjusting all these parameters, that affect the rate and amount of digestion of starch granules, in order to overcome limitations (e.g as stabilizer) and to fulfil novel approaches.

The uses of starch are numerous and being a natural polymer has been primarily utilized as a filler, a thickener, a sizing agent and a stabilizer due to its availability, low cost and biodegradability. In order to implement starch is such applications (Dong et al., 2022; Lin et al., 2022; Torres & De-la-Torre, 2022; Troncoso & Torres, 2020). a series of physical, chemical, genetical, and enzymatical modification methodologies have been proposed (Maniglia et al., 2020).

Physical treatment is among the most practical and environmentally benign techniques for creating novel nano-sized starches because of its ease, safety, and sustainability. Generally, starch can be physically treated to tailor-make its water solubility and granule size, which can lead to nano-particles or hydrophobic starch particles that have been effectively used to stabilize Pickering emulsions (Bu et al., 2020; Ko & Kim, 2021; Saari et al., 2017; Timgren et al., 2013).

Food-grade nano-particles can be produced using several different physical methods, such as irradiation, anti-solvent nano-precipitation, microemulsion, electrospinning or electrostatic spraying mechanical treatments employing extrusion, high pressure homogenization, ultrasonication and ball milling (Akhavan & Ataeevarjovi, 2012; Apostolidis & Mandala, 2020; Chutia & Mahanta, 2021; Dong et al., 2021; Duyen & Van Hung, 2021; Huang et al., 2022; Lin et al., 2022). The range for applications is very wide, with environment-friendly "green" based SNPs being used as fluorescent indicators and probes for biomedical applications, chemical sensing and food packaging, due to their ease of preparation, low cost, and efficient fluorescence emission (Chao et al., 2020; Guida et al., 2021; X. Liu et al., 2018; Qiu et al., 2019; Shibata et al., 2022; Yan et al., 2015).

Herein, we developed a novel sequential three-step physical process consisting of: hydrothermal gelatinization, nano-precipitation and ultrasonic treatment. During the first step, the RS starch granules were treated with water in an autoclave reactor. The heating process promotes gelatinization of the starch, increases the water solubility, the water binding, and the emulsion capacity, based to the temperature and the time of the treatment (Dundar & Gocmen, 2013). The effect of high temperatures in increasing swelling power and solubility has been noted in RS produced by Job's tears starch (Q. Yang et al., 2021), whereas in pea starch, high temperature treatment has been found to promote the formation of crystalline regions, as shown by the X-ray diffraction (Zhou et al., 2019). Although the digestion kinetics are out of the scope of the current work, it should be noted that recent reports suggest that hydrothermal autoclave treatment impacts positively the digestibility of starch (Akanbi et al., 2019). The second step of the physical process involved the nanoprecipitation of the gelatinized starch by adding ethanol as the non-solvent. Nanoprecipitation has been applied to a multitude of starch varieties, including waxy corn, potato, sweet potato high amylose corn, and pea (Qin et al., 2016). It is however known that during nanoprecipitation there is strong tendency towards agglomeration of the individual nanoparticles additional treatment is required to obtain uniformly distributed nanoparticles. To this, the third step of our approach was to treat the agglomerated nanoparticles, produced by the nanoprecipitation of the hydrothermally gelatinized starch, with ultrasounds. Combining nanoprecipitation and ultrasonication in processing of starches has been proposed as an efficient and low-cost option (Chang et al., 2017; Noor et al., 2022; R. Wang & Zhou, 2022). Ultrasonic treatment of starches has reportedly a beneficial impact to the physical properties of RS 2 type starches (Noor et al., 2021) and affects the crystallinity of the starch (Babu et al., 2019; Noor et al., 2021; H. Wang et al., 2020; Q. Y. Yang et al., 2019) without prompting damage (Hu et al., 2014; J. Zhu et al., 2012).

Collectively, our three-step physical process combines all the major advantages of the three individual physical processes. To the best of our knowledge, such an approach has not been applied to RS2 type starches. Our findings provide a better understanding of the mechanisms taking place during size reduction of starch particles through physical processing methods.

2. Materials and methods

2.1. Materials

High amylose maize starch (Hi-Maize 260®) was kindly provided by Ingredion Incorporated (Manchester, UK). The amylose amount was 65.2%, calculated by the method described in Subsection 2.3. and its moisture content was 12.44% w/w calculated using the AACC standard method (AACC, 2000). Absolute ethanol (98%) was obtained from Sigma-Aldrich and Milli-Q water was used for all the experiments.

2.2. Preparation of physical starch nano-particles via autoclaving (heat gelatinization) and precipitation-ultrasonication

Starch nano-particles were prepared using a similar method to the one previously described by Saari et al. (2017), with slight modifications (Saari et al., 2017). In particular, High amylose maize starch suspension (5%, w/v) were prepared by adding dry starch in distilled deionized water under mechanical stirring (RCT Basic S1 Digital Hot Plate Magnetic Stirrer, IKA®-Werke GmbH & Co. KG, Germany), at a speed of 1000 rpm, at room temperature (27 ± 1 °C). The starch suspension was transferred to an autoclave reactor with bomb geometry. The reactor was placed in a preheated oven at 150 °C and gelatinized for 30 min, starting from the time the suspension reached equilibrium according to the thermocouple's indication. After heating, the autoclave was transferred in an ice bath for 5 min in order to cool down. The gelatinized starch paste was then placed in a beaker and stirred at 1500 rpm using an IKA Eurostar digital stirrer (IKA Labortechnik Janke & Kunkel, Staufen, Germany).

Then, the antisolvent ethanol was poured dropwise into the agitated starch solution at a concentration of 1:1 for precipitation to take place, and the solution was left for 2 h under stirring. The slurry was centrifuged at 9000 rpm for 10 min at 4 °C (Hettich Universal 320-R, Germany). Next, the sediment starch nano-particles were freeze-dried at −60 °C for 48 h using a freeze dryer (MC4L, UNICRYO, Germany) and pulverized using a mortar and pestle; the resulting nano-particles were named aggregated-SNPs (a-SNPs).

In the next step, the produced a-SNPs were dispersed in Milli-Q water to create 1% w/v dispersion. Subsequently, the produced dispersion was homogenized in an ice bath using ultrasound treatment for different time intervals, up to 75 min (15 min, 30 min, 45 min, 60 min, 75 min), to control particle size. Specifically, ultrasonication was conducted using a probe sonicator (Sonopuls 3200, Bandelin Gmbh & Co, Berlin, Germany) operating at an amplitude of 40%, pulsation 3 s on/3 s off. Notably, particle samples processed for 30 min and 60 min were named a-SNPs 30 min and US-SNPs respectively. Ultrasonicated samples were freeze-dried to obtain dry samples for characterization.

2.3. Amylose content

The amylose content of native untreated starch and starch nanoparticles was determined using a concanavalin A method using the Megazyme amylose/amylopectin assay kit (Megazyme Ltd., Bray, Ireland). The amylose content was determined using the Megazyme equation (Eq. (1).) and by measuring the absorbance of the sample at 510 nm using a UV–Vis scanning spectrophotometer (Shimadzu, UV-2600, Kyoto, Japan).

$$Amylose\ content = \frac{Absorbance\ (Con\ A\ Supernatant)}{Absorbance\ (Total\ Starch\ Aliquot)} \times 66.8 \quad (1)$$

2.4. Particle size distribution

Particle size distribution of native starch and nano-particles was determined, using Dynamic Light Scattering (DLS) (Zetasizer nano Zs, Malvern Instruments Ltd., Worcestershire, UK) (Jeong & Shin, 2018). Water and starch have refractive indices of 1.33 and 1.53, respectively, while the absorbance of starch granules was 0.1. The particle size was reported as the mean hydrodynamic diameter (Z-average) for the starch samples at a concentration 0.01% w/v in Milli-Q water. Furthermore, we studied the decomposition of agglomerated particles as a function of time using ultrasonication for a time interval of 15–75 min. Each measurement was repeated three times.

2.5. Zeta potential measurements

The zeta-potentials of starch dispersions in Milli-Q water (0.01% w/v) were measured at 25 °C using a laser Doppler electrophoresis apparatus (Malvern Nano-Zetasizer ZS, Worcestershire, UK). All measurements were performed in triplicate for each sample.

2.6. Fourier transform infrared spectroscopy analysis (FTIR)

The infrared spectra of samples were acquired using a JASCO 4200 Type A Fourier transform infrared spectrophotometer (Jasco, Easton, MD, USA) that can identify any structural changes. The FTIR spectra were obtained within a wavenumber range from 400 to 4000 cm^{-1} and a resolution of 4 cm^{-1}, using the KBr pellet technique in Transmittance mode. The samples were combined with dried FTIR-grade potassium bromide (10 mg sample to 300 mg KBr) using an agate mortar and pestle, and the mixtures were pressed to form disk shape pellets at 10 tn/cm^2 using a manual, hydraulic pressure system (PE-MAN, Perkin Elmer, Germany).

2.7. Swelling power and water solubility

The solubility and swelling power of starch samples were analyzed by the procedure followed by (Aytunga et al., 2010; Mandala & Bayas, 2004) with slight modifications. Starch suspensions (2% w/v in Milli-Q water) were placed in 250-mL DURAN® glass bottles to prevent evaporation. The samples were next heated in an oil bath in a Temperature range of 50 °C–140 °C, with measurements recorded every 10 °C. The total heating time was 30 min under stirring (300 rpm) using an RCT Basic S1 Digital Hot Plate Magnetic Stirrer (IKA®-Werke GmbH & Co. KG, Germany). After gelatinization, the samples were allowed to equilibrate for 30 min at room temperature and then centrifuged at 5000 rpm for 15 min at 4 °C. The precipitate was separated by centrifugation from the supernatant and weighted (W_p). The dry solids in precipitated paste W_{ps} and supernatant W_s were estimated after drying both phases at 130 °C for 1 h in an air oven (Memmert, Schwabach, Germany). Before weighing the glass Petri dishes that contained the samples, samples were stored in a desiccator for 30 min. The fraction of dry mass of solubles in supernatant to the dry mass of whole starch sample W_o is expressed as solubility, and calculated with Eq. 2

$$Solubility = \frac{W_s}{W_0} \times 100\ \% \tag{2}$$

The ratio of the weight of swollen starch granules after centrifugation (g) to their dry mass (g) is expressed as swelling power and calculated with Eq. (3).:

$$Swelling\ Power = \frac{W_p}{W_{ps}} \tag{3}$$

2.8. Crystallinity of starch particles using X-ray diffraction

XRD analysis of native starch, a-SNP and SNP was performed as previously described (Apostolidis et al., 2021; Apostolidis & Mandala, 2020). For the subsequent analysis, an advanced X-ray Diffractometer (D8 Adv., Bruker, Germany), operating at 40 mA and 40 kV, was employed. Samples scanning using Cu Ka irradiation with a wavelength of 0.1542 nm as the X-ray source, was firstly applied. The X-ray generator was set to run at a diffraction angle (2θ) of 3°–35° with a step size of 0.05°/sec. In brief, the degree of crystallinity of a sample, based on the XRD pattern, was evaluated using the software Bruker Diffrac. Eva Version 3.1. Firstly, an automatic plot of the baseline of the curve (black line) and the background of the crystalline peaks (red line) was designed. Subsequently, the white area of the crystalline peaks along with white and grey total area of the peaks were calculated, as shown in Supplementary Fig. 1. The degree of crystallinity was calculated using Eq. (4).

$$\%\ crystallinity = \frac{area\ of\ crystalline\ peaks}{total\ area\ of\ the\ peaks} \times 100 \tag{4}$$

2.9. Small angle X-ray scattering (SAXS)

We conducted the SAXS experiments with the SAXSpace small angle X-ray camera from Anton Paar (Graz, Austria). The set-up and standard data reduction procedures are described (Sanver et al., 2020). Briefly, we used a line focused collimation X-ray beam with the beam length of 20 mm and 0.5 mm width. The sample to detector distance of around 317 mm was used, although the exact distance was obtained using silver behenate powder. Each sample was put into 1.5 mm capillary and exposed for 3600 s. The instrument was equipped with a sealed-tube Cu anode X-ray generator, operated at 40 kV and 50 mA, producing X-rays at wavelength $\lambda = 0.154$ nm. The setup was also operated at high intensity mode providing us with minimum accessible scattering vector value, q_{min} of 0.12 nm^{-1} ($q = 4\pi/\lambda \sin(\theta)$, where 2θ is the scattering angle). All the SAXS experiments were performed 25 °C.

The experimental scattering profiles were modelled using a unified equation described by Beaucage and co-workers (Beaucage, 2004; Beaucage & Schaefer, 1994). The model comprised of functions describing scattering from starch granules at different structural levels. The power law with exponential functions are used to explain the decay behavior at ultra-small angles and the Lorentzian functions are applied to simulate the diffraction peaks from lamellae and the interhelical correlations. The general form of the unified function can be represented according to Eq. (5).

$$I(q) = \sum_{levels} B_i\ exp\left(\frac{-q^2 R_i^2}{3}\right)\left\{\frac{\left[\mathrm{erf}\ \left(qR_i/\sqrt{6}\right)\right]^3}{q}\right\}^p + \frac{L_i}{1+\left[\frac{(q-q_i)}{w}\right]^2} \tag{5}$$

In the above equation, the first term accounts for the decay in the scattering intensity with two structural limits; the low-q limit is considered by the error function and the high-q limit is described by exponential functions. Both are associated with characteristic radius of gyration R_i. This characteristic length also determines the inflexion point where two Porod decay rates are identified. The second term describes the broad diffractions peaks. Two Lorentzian terms were used, the first one simulates the diffraction from lamellar spacing accounting for alternating amorphous and semi-crystalline domains of amylopectin at around 0.4 nm^{-1} (equivalent to 15.7 nm). The second Lorentzian peak function simulates the diffraction from the interhelical correlations in B-type starch. This peak occurs at around 3.9 nm^{-1} (equivalent to 1.6 nm spacing).

The average d-spacing (d) between the polymer aggregates was estimated from the peak position (q_0). according to the Bragg equation Eq. (6).

$$d = \frac{2\pi}{q_0} \tag{6}$$

The average thickness of the polymer aggregates was measured by

using the Scherrer equation (Eq. (7)), where K is the shape factor and w is the broadening of the correlation peak (Maurya et al., 2019).

$$h = k^* \frac{2\pi}{w} \quad (7)$$

2.10. Steady-state and time-resolved fluorescence

Three different samples were prepared and analyzed by steady-state and time-resolved fluorescence: the untreated nano-starch, as well as the nano-particles prepared by ultrasonication for 30 and 60 min. Each nano-starch powder sample was dispersed in Milli-Q water at a final concentration of 0.01 w/v using mild magnetic stirring for 30 min before measuring. Each dispersion sample (3 mL) placed in a quartz cuvette (1 cm path length). Steady-state emission spectra were recorded on a Horiba GL3-21 Fluorolog-3 Jobin-Yvon-Spex spectrofluorometer (Horiba, Kyoto, Japan), equipped with a 450-W Xenon lamp as the excitation source and a TBX photomultiplier (250–850 nm) as the detector, for photoluminescence (PL) measurements. Starch nano-particles were excited at 320 nm. Data were recorded and collected via the Horiba Fluorescence V3 software (Horiba Ltd., Kyoto, Japan). For the pico-second time-resolved fluorescence spectra, a time-correlated single-photon-counting (TCSPC) method via a Fluorohub single-photon counting controller, a laser diode as an excitation source (NanoLED, 376 nm, pulse duration <200 ps), and a TBX-PMT detector (250–850 nm) all by Horiba Ltd., Kyoto, Japan was applied. Data were recorded and collected with the Data Station software, whereas the lifetimes were determined by the Data Acquisition Software (DAS), all provided by Horiba Scientific, Piscataway, NJ, USA.

2.11. Stability of starch using thermogravimetric analysis (TGA)

TGA is typically used to assess the thermal stability of different starch samples by measuring the weight variations upon progressing temperature rise. Characteristically, TGA was performed for dried samples (~6 mg) under nitrogen gas circumstances in order to establish an inert atmosphere in the chamber, with a flow of 20 mL/min, and the samples were heated from 25 °C to 600 °C at a heating rate of 10 °C/min using a thermogravimetric analyzer (TGA/DTA model, Mettler Toledo, Schwerzenbach, Switzerland).

2.12. Contact angle measurements

The sessile drop method was used to determine the contact angles of native starch and nano-starch using the OCA 20 drop-shape tensiometer (Data Physics Instruments, GmbH, Germany), equipped with a high-speed camera, a micro-syringe and a Peltier cooling system, ensuring that measurements can be taken at a constant temperature of 25 °C. The particles were pelletized in a hydraulic press under 6 metric tons of pressure to create a suitable substrate surface, and placed in a rectangular optical glass cell. Milli-Q water dripped using a high precision micro-syringe system (Hamilton 500 μL DS 500/GT) by a straight stainless-steel dossing needle with a 0.52 mm outer diameter and 0.26 mm internal diameter was used to generate a sessile drop (5 μL, at a rate of 2 μL/s) onto the particle disc surfaces (about 2 mm thick). For determining the contact angles, a high-speed camera attached on the tensiometer captured the change of water droplet shapes at a rate of 10 frames per second, while SCA software was used to fit the droplet contour. The droplet profile was calculated using Young-Laplace equation.

3. Results and discussion

3.1. The size of nano-particles

Initially, the high amylose corn starch (Hi-Maize 260®) was subjected to hydrothermal gelatinization in an autoclave reactor. The starch was mixed with water at different concentrations and the temperature and processing time were studied. In principal, a high temperature is required in order to generate pressure inside the autoclave reactor. We found that above 160 °C the starch was quickly converted to a brown suspension indicating decomposition, while it was found to be stable at 150 °C for heating periods sufficient to promote gelatinization. More specific, keeping the mixture at 150 °C for 30 min resulted in full gelatinization. Heating for longer periods didn't improve further the gelatinization, whereas the starch started to degrade after 1 h at 150 °C. Low quality gelatinized mixtures were observed at lower temperatures even at longer heating periods.

After, nano-precipitated starch was produced via the addition of ethanol, collected via centrifugation and freeze-dried. In details, in the starch mixtures gelatinized at 150 °C for 30 min in the autoclave reactor the non-solvent was added dropwise under vigorous stirring at room temperature. Ethanol was selected as the non-solvent since it is biocompatible in contrast to other solvents (e.g. acetone). Further, slow addition of ethanol was prepared since fast addition of the solvent produced very inhomogeneous mixtures. After the dropwise addition of ethanol the mixtures were centrifuged until the separation of the solid from the liquid.

Finally, the isolated nano-precipitated starch powders were redispersed in water and treated with ultrasounds. Herein, a probe sonicator was used and the suspensions were sonicated at different amplitude and time intervals. Up to 40% amplitude we were able to sonicate the suspensions for prolonged periods, up to 2 h, without promoting degradation and ensuring appropriate cooling of the mixture. At lower amplitude less homogeneous dispersions were evident, namely larger lumps were present.

The particle size and size distributions of the nano-precipitated starch after the hydrothermal gelatinization and the freeze-drying processes were investigated by Dynamic Light Scattering (DLS). First we used a very low concentration of starch (0.1% w/v), which was gelatinized at 150 °C for 30 min and nanoprecipitated by ethanol. From the DLS analysis we witnessed displayed two peaks concerning the distribution of the particles, a major at ~200 nm and a minor at ~1 μm. Afterwards, the nanoprecipitated starch was ultrasonicated at 40% amplitude for different time intervals and a uniform population of ~200 nm was recorded. Then, we increased the concentration of starch up to the critical point of getting a gel after the hydrothermal gelatinization. Accordingly, above 6% w/v gels were produced and thus we couldn't proceed to the nanoprecipitation stage. Therefore, the maximum concentration of starch was as high as 5% w/v. The hydrothermally gelatinized 5% w/v starch mixture was then nanoprecipitated by ethanol and collected by centrifugation. After redispersion in water it was ultrasonicated at different time intervals with 40% amplitude. The particle size distribution of the ultrasonicated samples derived by the hydrothermal gelatinization/nanoprecipitation steps is depicted in Fig. 1. The DLS graph of the nanoprecipitated 5% w/v gelatinized starch displayed two peaks concerning the distribution of the particles, a major at ~200 nm and a minor at ~5 μm, in analogous fashion to the nanoprecipitated 0.1% w/v gelatinized starch. According to this observation it is evident that a 50-fold increment to the concentration of the gelatinized mixture affords the same sized nanoprecipitated particles. Furthermore, the initial high amylose starch is composed of large granules ~8 μm (Apostolidis & Mandala, 2020), and we assumed that the nanoprecipitated ~5 μm particles could be indicative of agglomeration of the smaller ones (~200 nm). In this essence, ultrasonication could be a potential physical treatment towards homogeneous starch nano-particles. Evidently, upon ultrasonication the size of the starch nano-particles was further reduced down to a uniform distribution (~170 nm, at 60 min ultrasonication), free of any agglomerates. In details, after 15 min of ultrasonication (US), the small peak noted at 5 μm was still evident. Notably, a similar size distribution was observed for the samples treated for a longer period of time (30 min), which was once again due to the agglomeration of the particles. After 60 min of US

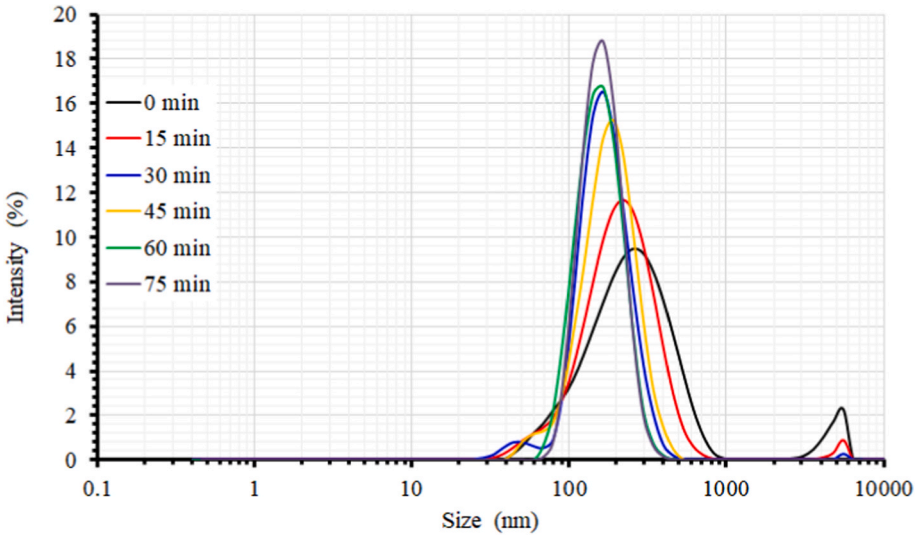

Fig. 1. Particle size distribution of SNPs and effect of ultrasonication exposure on size.

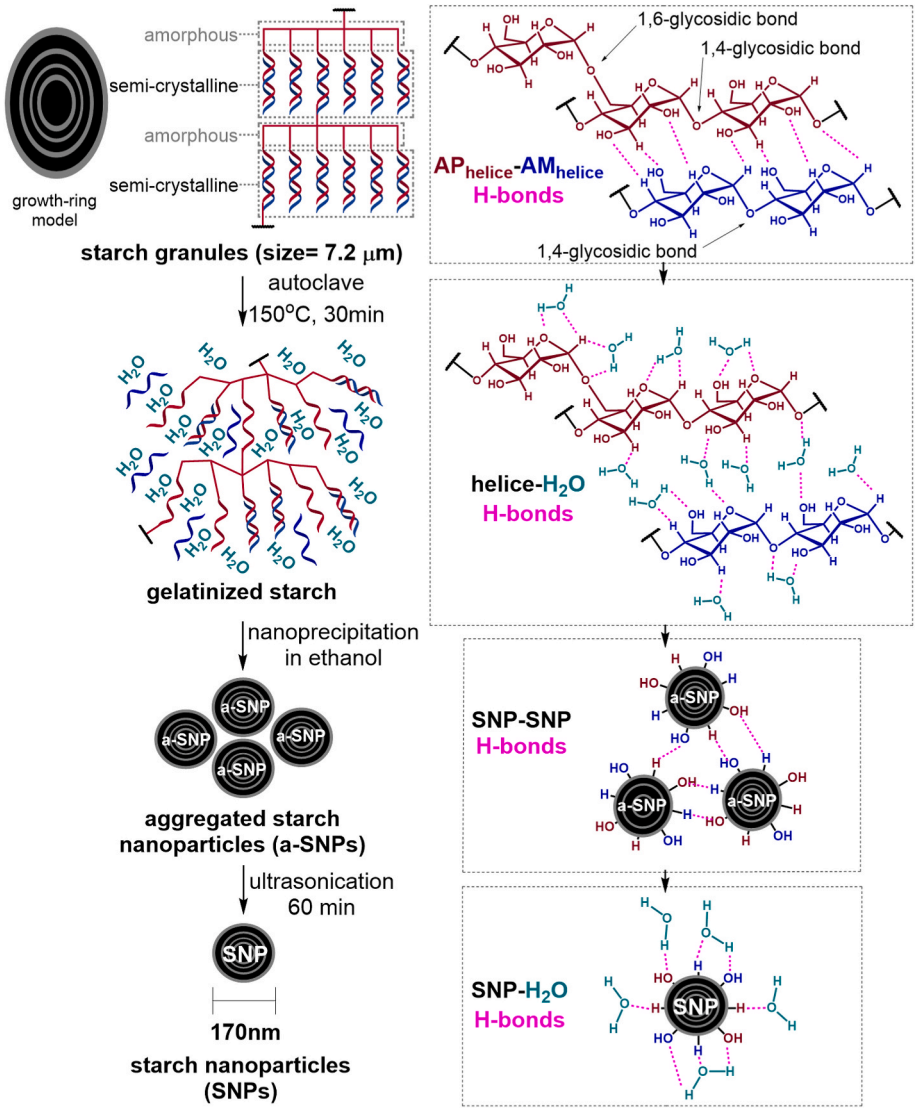

Fig. 2. Schematic illustration of the molecular behavior of the particles at all stages of the process of overall procedure for nano-particles formation.

treatment, the peak corresponding to the large particles (5 μm) disappeared, showing a unimodal distribution. The size distribution was effectively narrowed by ultrasonication over time; the hydrodynamic diameters of the ultrasound-treated nano-particles did not display a statistically significant difference between 60 min (169.9 nm) and 75 min (169.4 nm) of US treatment, and for this reason we considered 60 min as an appropriate time for full individualizing. To this, we denoted the as-prepared nano-precipitated starch nano-particles as agglomerated starch nano-particles (a-SNPs), while these produced via 60 min ultrasonication are considered starch nano-particles (US-SNPs). Summarizing, during the three-step physical process the initial large starch granules were changed to homogeneous SNPs, displaying a unimodal size distribution.

In Fig. 2, the molecular behavior of the particles at all stages of the processes was inferred schematically. Starch is composed by amorphous domains (around amylopectin branches) and semi-crystalline double helix (amylopectin-amylose) domains, stabilized through helix-helix hydrogen bonds. Upon the hydrothermal gelatinization step, water molecules were penetrating the starch granules and gradually displaced the helix-helix hydrogen bonds by forming helix-water hydrogen bonds. As a result, the granule got swollen and amylose leaches from the helix-helix semi-crystalline phase, mediating the gelatinization of the starch (Jenkins & Donald, 1998; Ren et al., 2021). During the addition of ethanol, which acts as a non-solvent, the precipitation of the formed a-SNPs resulted to the formation of agglomerates; this phenomenon is attributed to particle-particle hydrogen bonds. Finally, the ultrasonic treatment disrupts the weak particle-particle hydrogen bonds and uniformly distributed SNPs were released. Collectively, the large numbers of oxygen, hydroxyl and hydrogen groups being present in starch tend to reform the supramolecular connections in its structure, namely via the formation of different types of hydrogen bonds (Qiu et al., 2016; Wei et al., 2014). In this regard, it is noteworthy that the nano-precipitation method efficiently reduced the particle size of the initial starch, although the derived nano-particles had a tendency to agglomerate, previously reported for quinoa and high amylose starches (F. Jiang et al., 2022; Ruan et al., 2022). According to our findings, we stress that a simple treatment of such a-SNPs with ultrasounds caused physical breakdown of the nano-particle aggregates, driving the particle size distribution to grow narrower. The question is whether an ultrasonication caused further structural changes to starch particles such as crystallinity changes, which will be discussed later on.

Digital photos of starch suspensions under the Tyndall effect are shown in Fig. 3. Interestingly, the Tyndall effect of starch nano-particles is used as a light scattering signaling readout identification technology for naked-eye detection. This technique has been successfully used in nano-starch suspensions, where, when the suspension containing particles was illuminated by a light beam, the Tyndall effect could be detected through light scattering induced by the scattered particles (Andrade et al., 2020; Boufi et al., 2018). Characteristically, light traveled through pure water without scattering and no Tyndall effect was noticed, but in the native starch dispersion, a conical beam induced by Tyndall scattering was observed. In the case of a-SNP particles, the laser beam was effectively blocked from passing through, resulting in a narrow light path with a conical beam that presented a lower transmittance. The area of the conical beam shrank as the ultrasound time increased, while the optical path lengthened, while starch suspension's turbidity and transparency changed. A strong and long light path was detected when the time was prolonged to 60 min, with an unobstructed laser light route showing the presence of nano-sized particles. To summarize, adding ultrasound treatment after nano-precipitation, is an effective approach for producing tailor-made sized nano-particles, whereas the Tyndall effect can be used as a rapid method for nano-particle identification.

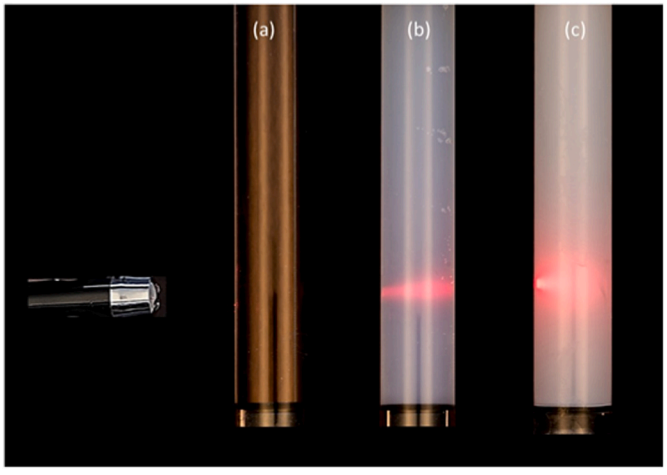

Fig. 3. Digital photo showing the Tyndall effect in different systems: a) in water, b) US-SNPs, C) a-SNPs.

3.2. Amylose content

Amylose content is an important factor affecting starch's structural characteristics and its digestion pattern (Fitzgerald et al., 2011; Zhao et al., 2022). A major drawback of this method is the frequent overestimation of the amylose concentration of starch, because of the branch-chains of amylopectin that bind iodine. An alternative colorimetric approach is based on dual wavelength measurements (T. Zhu et al., 2008). However, despite the efforts to produce more precise measurements, these two colorimetric techniques can only assess the apparent amylose content (AAC), while a Concanavalin A (ConA) based assay has been proposed as an alternative that allows us to evaluate true amylose content (TAC) (Y. Li et al., 2022).

The true amylose content (TAC) of High amylose corn starch was measured at 65.2%, a value quite similar to its estimated apparent amylose content (AAC) (59.5%), as described in a previous work by members of our research team (Apostolidis & Mandala, 2020). The TAC estimation was calculated from the UV spectra as depicted in Fig. 4. Concerning the a-SNP samples, a smaller amount of TAC was found, equal to 39.4%. The reduction in amylose content could be due to amylose leaching as a result of hydrothermal treatment, causing breaking of the hydrogen bonds in the helices leading to the release of amylose. This process leads to the creation of amylose-amylose and amylose-amylopectin interactions leading to under estimation of TAC. An analogous observation has been reported for hydrothermally processed talipot starch (Aaliya et al., 2022). Crystallinity changes are discussed later on to find out structural changes of RS according to the autoclave, precipitation and ultrasonication processes that were used.

3.3. Zeta potential

The zeta-potential (ζ) is an effective measurement related to the stability of the colloid starch dispersions (Dai et al., 2018; Ullah et al., 2018). Surface charge controls the dispersion and aggregation, namely an increment to the absolute value of the zeta potential is indicative of increased surface charge and hence colloid stability and vice versa. All our samples displayed negative zeta potential values, as presented in Fig. 5, indicative of non-chemically functionalized starch derivatives dispersed in water (Brust et al., 2020; Pérez & Bertoft, 2010). Characteristically, the zeta potential of the US-SNPs gradually shifted to more negative values as a result of the prolonged ultrasonic treatment. In details, the zeta potential value of the untreated starch was −13.34 ± 0.63 and after the two-step hydrothermal/nano-precipitation treatment the registered value for the isolated a-SNPs were found to be −14.4 ± 0.54 mV. Then, ultrasonication of a-SNPs for 60 min resulted to a zeta potential equal to −21.56 mV (US-SNPs). The gradual negative increment of the zeta potential dictated that the performed physical

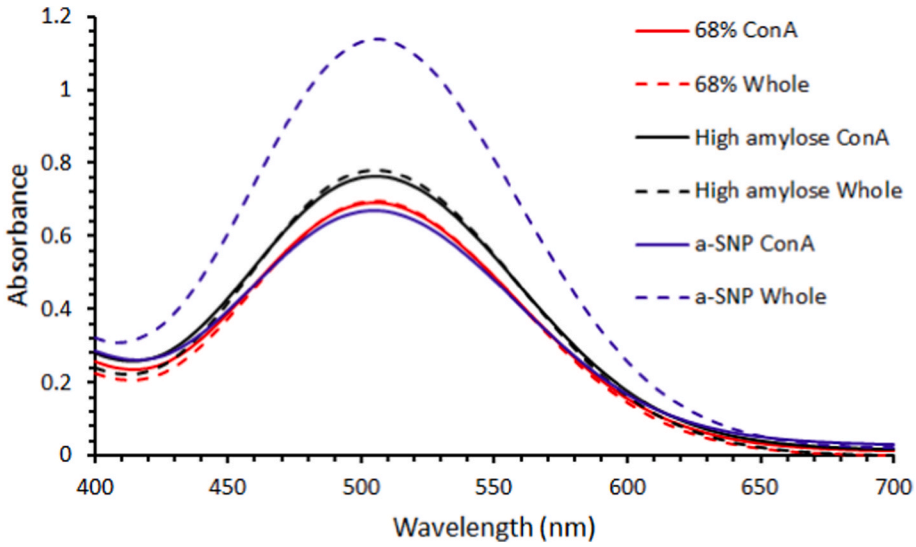

Fig. 4. UV spectra of amylose determination. [68% Con A: Con A-treated reference starch sample with 68% amylose; 68% Whole: Whole reference starch sample, 68% amylose; High amylose Con A: Con A-treated high amylose starch sample; High amylose Whole: Whole high amylose starch sample; a-SNP Con A: Con A-treated a-SNP sample; a-SNP Whole: Whole a-SNP sample].

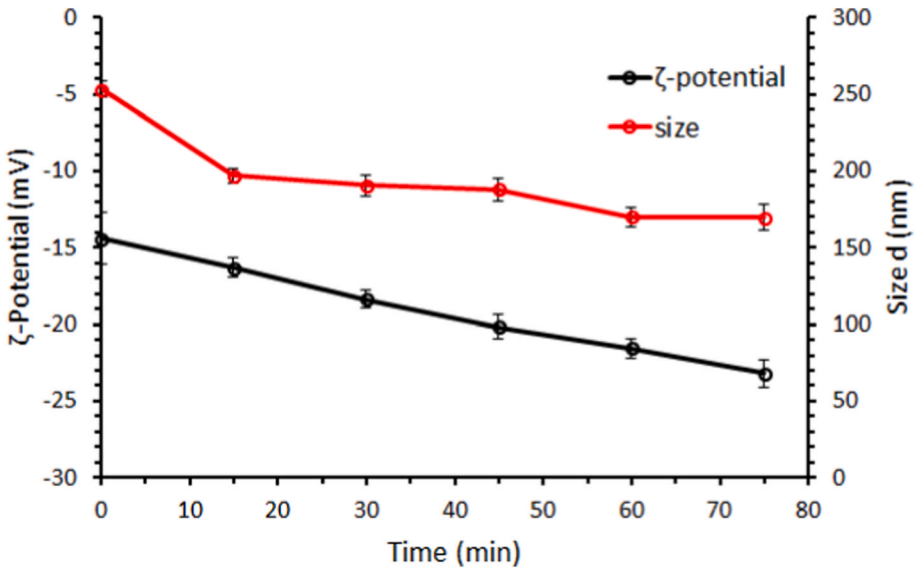

Fig. 5. Zeta potential and particle size with Ultrasound time.

treatments minimized the tendency of SNPs to self-aggregate due to van der Waals attractive forces at the particle-particle interfaces. Furthermore, the electrostatic repulsion was augmented, aggregation was minimized, and the hydrodynamic diameter was decreased. It is noteworthy that zeta potential values are obtained from the measured velocity of particles in an external electric field so called, electrophoretic mobility. Similar to the zeta potential values, the electrophoretic mobility data demonstrate a shift towards more negative values with physical treatment (see Supporting information). The enhanced zeta potential might be due to the increased electrostatic repulsion for the US-SNPs as a result of exposure of charged groups emerging from conformational changes caused by ultrasonication (Agi et al., 2019; Noor et al., 2022; Ullah et al., 2018; Zhang et al., 2022). However, it can also be partially due to the reduced hydrodynamic radius of the particles that encounter lower friction and hence, higher mobility when exposed to an external electric field. The most negative zeta potential value (−21.56 mV) recorded for the smallest US-SNPs (169.9 nm), is characterizing the system as moderately stable with time, blocking the fast particle aggregation. In contrast, the as-prepared SNPs (−14.4 mV, 252.8 nm) finally lead to clustered particles caused by increased attractive van der Waals forces. Concluding, the results indicate that the sequential hydrothermal gelatinization, nano-precipitation and ultrasonic processes efficiently produced nano-particles, resulting in good suspension stability and provides a correlation between the zeta potential and particle size.

3.4. Fourier transformation infrared spectroscopy analysis (FTIR)

The FTIR spectra were used to examine the molecular structure after native resistant starch was nano-precipitated and ultrasonically processed and the results are shown in Fig. 6. FTIR spectroscopy provided five main bands for each sample that were registered roughly in the same wavenumbers. Untreated starch, a-SNP, a-SNP 30 min and US-SNP showed characteristic bands at 3800-3000 cm^{-1} which are related to vibrational stretching of the O–H bond (free, inter and intramolecular hydroxyl groups) (Dong et al., 2022; Fang et al., 2002; Nain et al., 2022).

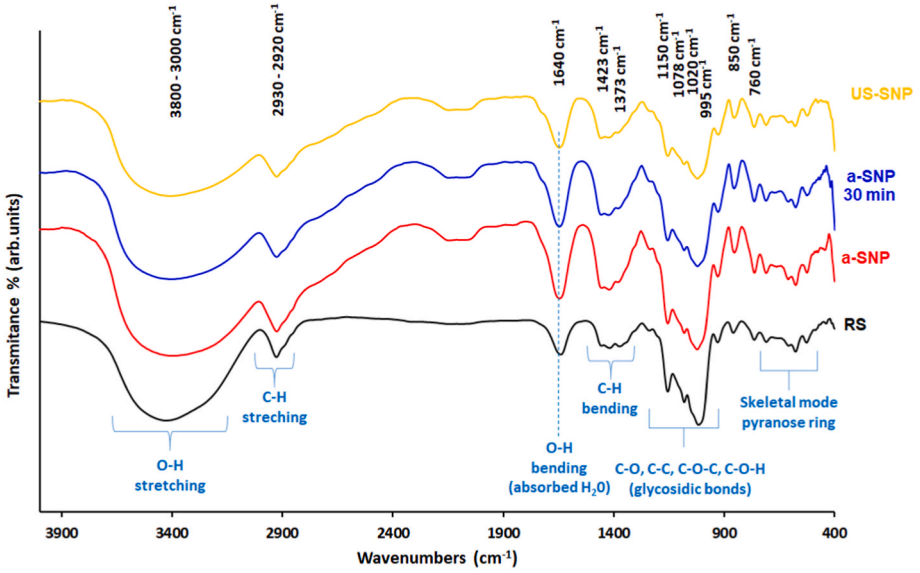

Fig. 6. Fourier transform infrared spectroscopy of high amylose (RS), a-SNPs, as-prepared a-SNPS after 30 min ultrasonication and the final US-SNPs.

In comparison to native starch, the peaks of O–H stretching shifted for all SNP samples to lower wavenumbers. This change revealed that the SNP's hydrogen bonds were stronger than those in the native starch granules which is in agreement with previous findings (Ahmad et al., 2020; Ma et al., 2007). The absorption bands at around 2930 cm^{-1} were characteristic to C–H asymmetric stretches associated with the pyranose rings of native and nano-starches. Additionally, the absorption band at 1640 cm^{-1} was observed, which is most likely a result of tightly bound water in the starch, as suggested by previous reports (Ahmad et al., 2020; Kaczmarska et al., 2018; Nain et al., 2022) and it does not demonstrate any obvious differences in the peak intensity after the size reduction of starch. Furthermore, the spectral region at 1450- 1300 cm^{-1} exhibits a pattern characteristic of C–H bending. In particular, the band at 1423 cm^{-1} is attributable to CH_2, whereas the one at 1373 cm^{-1} is associated with C–O–H bending vibrations (Kaczmarska et al., 2018). The IR band region at ~1200-900 cm^{-1} is of high interest since it includes bond vibrations that are sensitive to starch structure. However, these vibrations are highly overlapped, making the assignment of individual bands very difficult. Nevertheless, the main absorption peaks at 1150, 1078 and 1020 cm^{-1} can be attributed to the stretching vibrations of the C–O of the anhydroglucose ring while this at 930 cm^{-1} is assigned to the skeletal mode vibrations of the α-1,4-glycosidic linkage C–O–C group (930 cm^{-1}) (Nain et al., 2022; Q. Sun, Li, et al., 2014; Warren et al., 2016). Concomitantly, the IR band at 850 and 760 cm^{-1} represents the C–H of CH_2 deformation and C–C stretching respectively, while the region at 760-550 cm^{-1} is attributed to the skeletal mode of pyranose ring (Kizil et al., 2002; Warren et al., 2016).

In order to have an indication of the short range ordered molecular structure of the produced starches, the 995:1020 cm^{-1} peak ratio was calculated. The peak ratio values decreased after the SNP formation. In particular, native starch presents a value of 0.96 while all SNP samples present a value of 0.93. The aforementioned results are in good accordance with XRD analysis that follows, where a decrease in crystallinity was observed at SNP samples (15%–~12%), a phenomenon reported both for physically and chemically processed starches (Ahmad et al., 2020; Dong et al., 2022; Warren et al., 2016). All in all, FTIR spectroscopy is a helpful tool to validate the chemical integrity of the (nano) starch. Herein, it is evident that no chemical degradation mechanisms were taken place during nano-procedure and the final nano-particles are free of any oxidized chemical species (i.e. COOH and C═C groups).

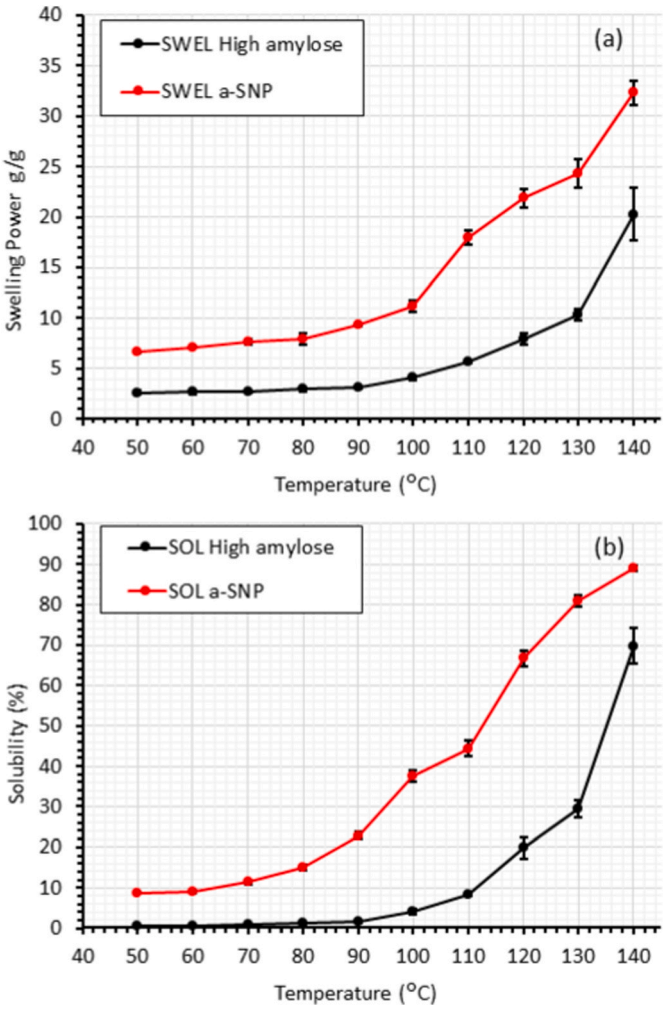

Fig. 7. a) Swelling power and b) solubility index of high amylose and a-SNP starches in a Temperature interval.

3.5. Swelling power and water solubility

The capacity of starch to absorb water at a specific temperature is known as swelling power. Initially, the swelling power profiles of native and starch nano-particles at different temperatures ranging from 50 to 140 °C are presented in Fig. 7 a. As it is observed, the swelling power of a-SNPS and Native starches increase with the increase in temperature. The breakdown of the extensive hydrogen bonding holding together the amylose and amylopectin in starch granules occurs in excess water and high temperatures, which destroy the crystalline areas and induce swelling of starch granules, leading to an in increase in the swelling power of starch. For native starch, a gradual increase in the swelling power behavior was observed at 100 to 140 °C. Comparatively, changes occurring in the swelling power of the studied nano-particle samples revealed that gradual increase in the swelling power behavior was observed at a temperature range of 90–140 °C. Remarkably, it should be noted that nano-particles have higher values of swelling power in all temperature ranges compared to untreated starch particles and exhibit a significant difference from each other ($p \leq 0.05$). This phenomenon is attributed to the decrease of amylose portion that we measured in a-SNPs, which denotes that the weak intermolecular interaction force leads to amylopectin's reduced moisture absorption and retention ability (Navaf et al., 2020; Xing et al., 2017). The increased swelling power of a-SNP samples when compared to native samples is attributed to the reduced amylose concentration within the amorphous regions, as a result of the nano-procedure approach, and the concomitant rise in the amylopectin content, which controls swelling. Afterall, the swelling power is often assumed to be predominantly a characteristic of amylopectin (J. Y. Li & Yeh, 2001; Xing et al., 2017).

For solubility, a similar pattern as a function of temperature was discovered for the starch swelling power (Fig. 7 b). When the temperature was raised to 140 °C, the a-SNP and untreated starches presented the maximum solubility value. Higher solubility values were found for a-SNPs compared to untreated starch, throughout the temperature spectrum. It is interesting that, at the lowest temperature of 40 °C, native particles presented practically no solubility, while a-SNPs presented values at around 10%. Moreover, at the highest temperature, a-SNPs had a 27.5% increase of solubility compared to the untreated. Native starch samples, in the temperature range of 50 °C to 90 °C, presented no solubility and showed an increase of around 1.57% during that range. Concluding, as the temperature increased from 50 to 140 °C, the swelling power and solubility of native starch and a-SNPs increased continuously, where remarkable differences between the two starches were found.

3.6. Crystallinity of starch particles using X-ray diffraction

Originally, the X-ray diffraction patterns of native starch, a-SNPS, and US-SNPs are presented in Fig. 8. The main peaks at about 5.4°, 17°, 20° and 23° (2θ) indicate that the structure of RS2 starch displayed patterns typical of B-type crystallinity, in accordance to previously published data of our research group (Apostolidis et al., 2021; Apostolidis & Mandala, 2020). The main peaks detected were comparable across all samples, demonstrating that particle size does not affect maize starch structure, while in parallel maintaining a B-type pattern albeit with lower crystallinity (Fig. 7). More specifically, the crystallinity measurement showed a value of 15.2% for the untreated starch, while a slight decrease was observed for the a-SNPs with a value of 12.4% and a value of 12.2% for US-SNPs. Additionally, for treated samples it is clear that ultrasounds had no impact on structure, with all the diffracted peaks presenting similar intensity. Since ultrasonic treatment is a relatively mild process, alteration of the crystal structure is not likely to occurred and this presumably explains analogous reports (Carmona-García et al., 2016; Falsafi et al., 2019; Monroy et al., 2018; Rahaman et al., 2021). This behavior could be explained by the treatment's influence of the lamellar array of starch granules. Generally, amylopectin determines the ordered crystalline parts of starch, while amylose determines the disordered amorphous regions (F. Jiang et al., 2022). Our samples were found to have decreased crystallinity, despite the fact that their amylose content was lower. We conclude that the decreased crystallinity is a synergistic phenomenon were contributing both the low amylose content and the reduced size of the particles. The latter is likely to be the critical factor (D. Liu et al., 2009).

3.7. Small angle X-ray scattering (SAXS)

The most common structural feature in starch granules appear to be a few nano-meters lamellar spacing arising from the alternating amylopectin amorphous and semi-crystalline domains. The SAXS peak relating to this structural feature typically occurs between 0.6 and 0.8 nm^{-1} (Luo et al., 2021). Such lamellar arrangement has been reported at very high intensities for normal maize or potato starches (Doutch & Gilbert, 2013). In our studies, the lamellar peak is pronounced well at 0.47 nm^{-1} for high amylose starch accounting for 13.6 nm spacing (Fig. 9). Although

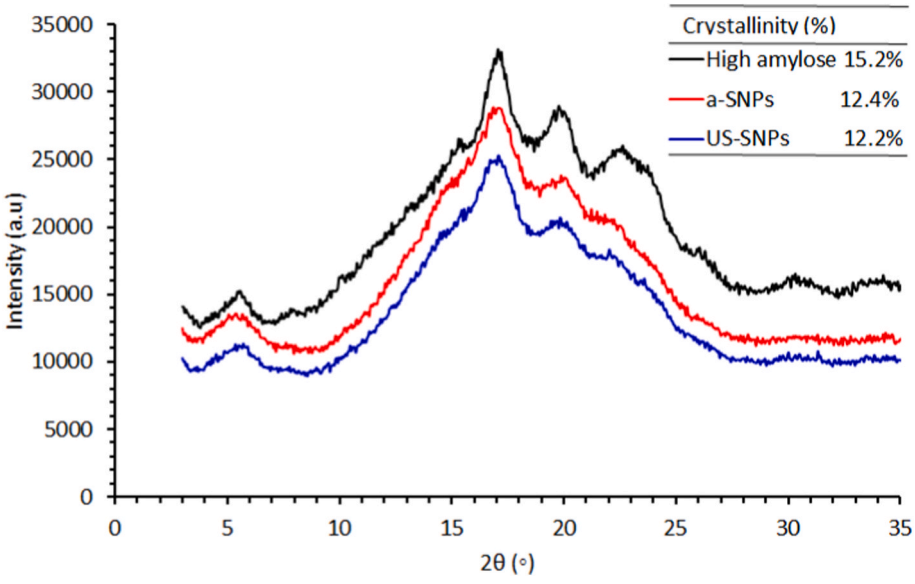

Fig. 8. X-ray diffraction patterns of High amylose, a-SNPs and US-SNPs.

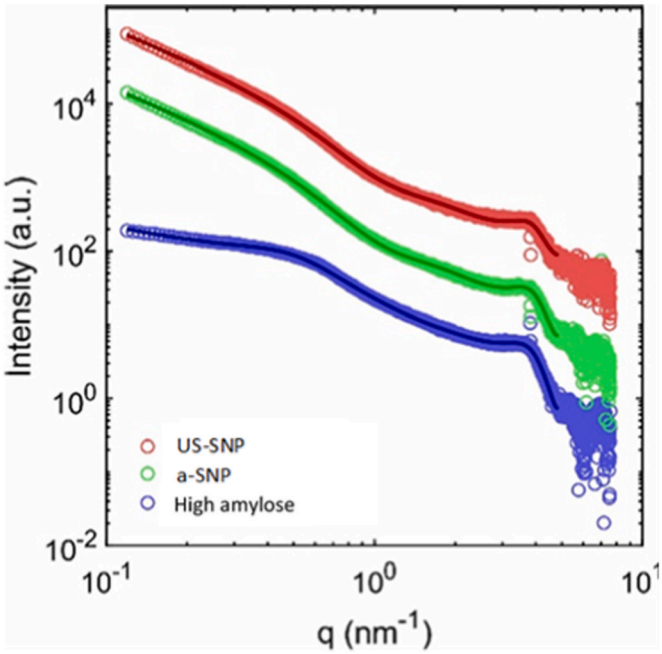

Fig. 9. The small angle X-ray scattering data; experimental data shown by open circles and the solid lines represent the simulated scattering curves according to the unified model. The two arrows represent the diffraction peaks at around 0.46 and 3.96 nm^{-1}, arisen from the lamellae and interhelical structures, respectively.

Table 1
Lamellar parameters obtained from SAXS.

Peaks	Parameters	Samples		
		High-amylose	a-SNP	US-SNP
Peak L	q_{peak} (nm^{-1})	0.4654	0.4654	0.4654
	width (nm^{-1})	0.2266	0.2290	0.2088
	d (nm)	13.499	13.499	13.499
	h (nm)	8.2505	9.6767	9.2538
Peak B	q_{peak} (nm^{-1})	3.8290	3.9106	3.9106
	width (nm^{-1})	1.6409	1.6067	1.6067
	d (nm)	1.6409	1.6067	1.6067
	h (nm)	3.3159	3.3866	3.3866

h: average thickness of semi-crystalline lamellae.
d: average d-spacing between polymer aggregates.

this peak is highly pronounced for non-treated starch, its intensity reduces considerably for a-SNP sample and completely disappears when ultrasound treatment is applied and presented in Table 1. This implies that the lamellar arrangement of amylopectin molecules almost disappears after nano-precipitation of the granules.

Another diffraction peak at x-ray scattering profiles is observed around 3.8 nm^{-1} which is a characteristic peak for B-type starch samples. The position of this peak remains almost the same for all samples. This peak accounts for the hexagonal arrangements of helices from hydrocarbon chains, correlates with interhelical distancing and is equivalent to 1.65 nm spacing. Its position remains nearly the same in all samples, demonstrating that the nano-precipitation or ultrasonic treatment does not influence the chain packing.

3.8. Steady-state and time-resolved fluorescence

Starch resembles a maximum absorbance at ~340 nm and negligible fluorescence in the solid state, therefore has been explored as a silent fluorescence matrix for light-emitting probes (M. Sun, Li, et al., 2014). Herein, dispersion of a-SNPs in water (0.01 w/v) and subsequent excitation at 340 nm revealed an intense broad fluorescence emission peak centered at 417 nm (Fig. 10). The recorded fluorescence lifetime for a-SNPs was best fitted with three exponential components ($\tau_1 = 2.75$ ns, 42.85%; $\tau_2 = 13.72$ ns, 31.81%; $\tau_3 = 400$ ns, 25.34%) giving a mean lifetime (τ_{av}) of 5.64 ns. We assume that the fluorescence emission properties of a-SNPs are a synergistic phenomenon of structural deformation, hydrogen bonding and particle size. As a result of the hydrothermal/nano-precipitation process, a-SNPs are able to form a dense H-bond network when dispersed in water (Fig. 2). The latter may induce a short-range charge delocalization responsible for the emerging fluorescence. Analogous photo-physical properties have been reported for other natural non-aromatic biomolecules favoring H-bond networks in water media (Pinotsi et al., 2016). Furthermore, subjecting the a-SNPs to ultrasonication for 30 min, the fluorescence emission increased by 14% and the peak maximum red-shifted by 7 nm (424 nm). Interestingly, the corresponding τ_{av} was found to be 5.56 ns, meaning it is practically unchanged. DLS studies suggested that a-SNPs are gradually disaggregated during the ultrasonic treatment. Dismantling of the SNP aggregates increased the fluorescence intensity as a result of less static quenching due to particle-particle interactions. Further, the coverage of the particles surface with water molecules explains the observed red-shift. Finally, at 60 min of ultrasonication the resulting US-SNPs displayed a further red-shift in the maximum of the fluorescence emission spectrum (428 nm) accompanied by a slight intensity increment (2%), while the τ_{av} calculated to be 5.62 ns. With the average fluorescence lifetime of a-SNPs and US-SNPs being practically unchanged, it is concluded that ultrasonication is mostly involved in dismantling the aggregated SNPs, which directly translated into an increment to the fluorescence emission intensity.

3.9. Stability of starch using thermogravimetric analysis (TGA)

The thermogravimetric analysis (TGA) curves for starch and SNPs are displayed in Fig. 11a. The TGA provided significant information about the thermal stability of starches. In particular, the TGA curve revealed similar behavior for the studied samples, containing two main weight loss steps which concern: a) the evaporation of the absorbed water at T < 120 °C indicating the dehydration of starch (weight loss ~ 10%) and b) the degradation of amylose and amylopectin which is related to the major weight loss (~60%) at ~ 280 °C–340 °C (Azad et al., 2022; Chinnasamy et al., 2022; S. Jiang et al., 2016). Furthermore, the TGA curves can also be used to determine the Tmax, or the temperature at which these starch biopolymers lose the most weight during thermal degradation, 300 °C for native and nano starches.

The first derivative of the TGA signals (DTGA) curve has two characteristic for starch samples features (Kumar Malik et al., 2022). These two peaks are the result of the absorbed water molecules escaping the starch network at 67 °C and the subsequent decomposition of the starch at 300 °C. It is noteworthy that US-SNPs presented a lower rate of 2nd degradation step, suggesting a slightly improved thermal resistance of the starch network (Fig. 11b). All in all, the prepared starch nano-particles follow the decomposition trend of the parent starch, proving that the particle dimensions were reduced (nano scale) without changing the chemical composition of the starch nano-particles This is, again, in agreement with the FTIR and XRD analysis.

3.10. Contact angle

Contact angle (CA) is a quantitative indicator of the wettability of a solid surface by a liquid, and it is a commonly used method for determining whether a solid surface is hydrophilic or hydrophobic. (Faille et al., 2019; Shahbazi et al., 2018). The contact angles for a-SNP and native starch were estimated to be 63.09° and 50.17° respectively, measured through water phase (Fig. 12). CAs larger than 90° have long been thought to be hydrophobic, owing to the water-material adhesion

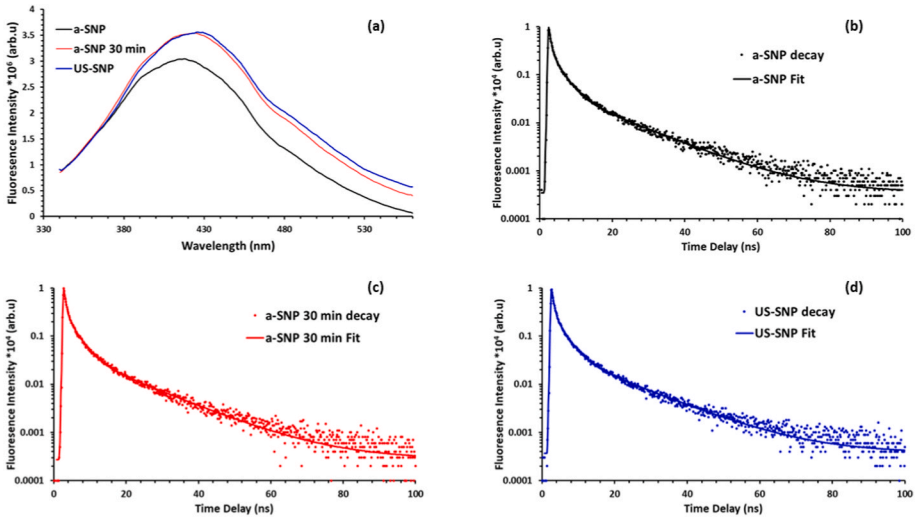

Fig. 10. (a) Fluorescence spectra of a-SNPs and (b), (c), (d) fluorescence lifetime decay spectra of as-prepared a-SNPS after 30 min ultrasonication and the final US-SNPs.

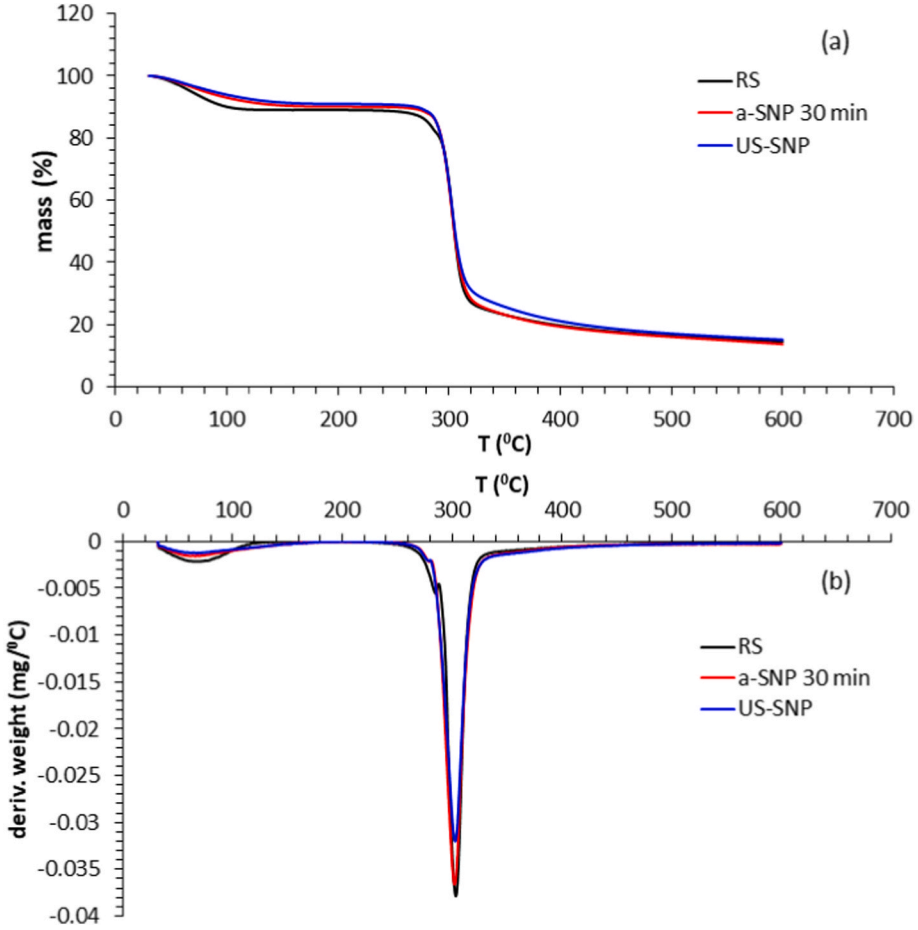

Fig. 11. TGA results (a) Weight loss of the composites, (b) Derivative weigh loss of composites.

interaction. The lower the contact angle, the better the wettability.

Native starch surface was replete of OH-rich macromolecules and it was possible to generate hydrogen bonds with water. These findings, when combined with the prior discussion of zeta-potential, show that reducing the particle size of native starch causes higher compensatory H-bonding connections between the SNPs matrix (a-SNPs), thus resulting in a bio-nanocomposite tablet with fewer accessible OH groups.

4. Conclusions

Herein, we proposed a sequential three-step physical process consisting of: hydrothermal gelatinization, nano-precipitation and ultrasonic treatment of Hi-Maize260®, an RS2 type starch. The sequential hydrothermal gelatinization/nanoprecipitation produced nano-sized RS2 particles, displaying two major populations of 200 nm and 5 μm,

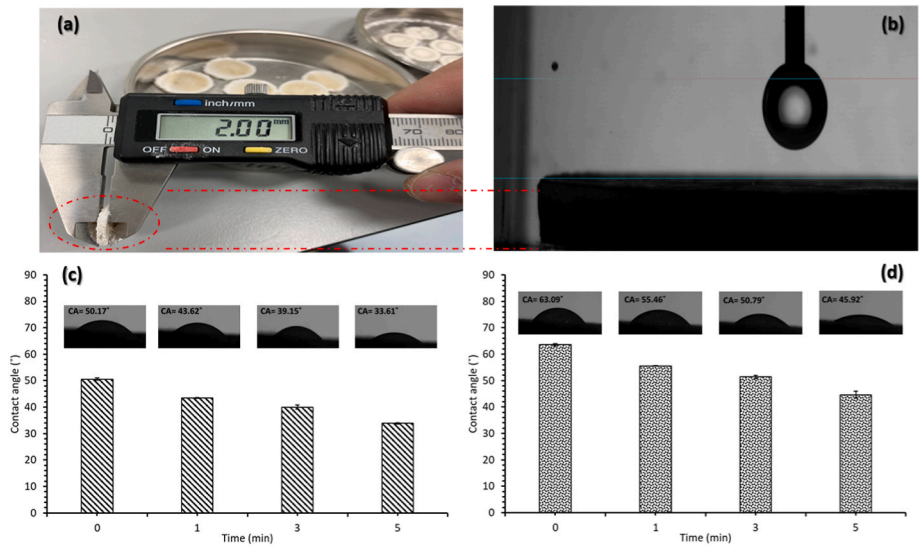

Fig. 12. Images of the prepared pelletized (disc) starch sample (A) and sessile drop on pelletized starch (B) Contact angle for High amylose (C) and a-SNP(D) at varied times.

while during the final step of ultrasonication uniform nanoparticles of 170 nm were isolated. We also showed that after nano-production, the amylose content was reduced from 65.2% to 39.4%, due to amylose leaching, as a result of hydrothermal treatment. Notably, a diminutive change in crystallinity was observed by XRD, while a slight decrease in the scattering intensity noticed in SAXS spectrum is likely to originate from the size reduction. Further, the nanoparticles were found to be chemically identical to the starting starch, since no new chemical species were identified by FT-IR spectroscopy, manifesting that no damage occurred during the three-step process. Furthermore, the solubility and swelling power behavior of the isolated nanoparticles improved as the temperature rises, as compared to the starting starch. The nanoparticles retained a hydrophilic behavior and displayed increased thermal stability. Notably, size reduction and dismantling of agglomerates reflected also to the increased fluorescence intensity. Summarizing, these results provide meaningful insights on how the physical properties of starch particles are affected during physical processing towards size reduction. This handy three-step physical process has the potential to contribute in new advances in the evolving area of starch-based Pickering emulsions.

CRediT authorship contribution statement

Eftychios Apostolidis: Conceptualization, Methodology, Validation, Investigation, Visualization, Formal analysis, Writing – original draft. **Anastasios Stergiou:** Investigation, Resources. **Dimitrios Kioupis:** Investigation, Resources, Formal analysis. **Amin Sadeghpour:** Investigation, Resources, Formal analysis, Supervision. **Paraskevi Paximada:** Investigation, Resources, Formal analysis, Supervision. **Glikeria Kakali:** Investigation, Resources. **Ioanna Mandala:** Conceptualization, Supervision, Writing – original draft, Writing – review & editing, Resources, Project administration, Funding acquisition.

Declaration of competing interest

The authors declare no conflict of interest and no competing financial interest.

Data availability

Data will be made available on request.

Acknowledgement

Part of the experiments were carried out at the University of Leeds in the School of Food Science and Nutrition, through the Scholarship of Mr. Apostolidis Eftychios: Greek-British Cooperation for short-term mobility in the United Kingdom. The Greek State's Scholarships Foundation (IKY) and the British Council in Greece are gratefully acknowledged for financially supporting part of this work.

Appendix A. Supplementary data

Supplementary data to this article can be found online at https://doi.org/10.1016/j.foodhyd.2022.108412.

References

AACC. (2000). *American association of Cereal Chemists. Approved methods Committee* (Vol. 1). Approved Methods of the American Association of Cereal Chemists.

Aaliya, B., Sunooj, K. V., Navaf, M., Akhila, P. P., Sudheesh, C., Sabu, S., Sasidharan, A., Sinha, S. K., & George, J. (2022). Influence of plasma-activated water on the morphological, functional, and digestibility characteristics of hydrothermally modified non-conventional talipot starch. *Food Hydrocolloids, 130*, Article 107709. https://doi.org/10.1016/J.FOODHYD.2022.107709

Agi, A., Junin, R., Gbadamosi, A., Abbas, A., Azli, N. B., & Oseh, J. (2019). Influence of nanoprecipitation on crystalline starch nanoparticle formed by ultrasonic assisted weak-acid hydrolysis of cassava starch and the rheology of their solutions. *Chemical Engineering and Processing - Process Intensification, 142*, Article 107556. https://doi.org/10.1016/J.CEP.2019.107556

Ahmad, M., Gani, A., Hassan, I., Huang, Q., & Shabbir, H. (2020). Production and characterization of starch nanoparticles by mild alkali hydrolysis and ultrasonication process, 10(1) *Scientific Reports 2020, 10*(1), 1–11. https://doi.org/10.1038/s41598-020-60380-0.

Akanbi, C. T., Kadiri, O., & Gbadamosi, S. O. (2019). Kinetics of starch digestion in native and modified sweetpotato starches from an orange fleshed cultivar. *International Journal of Biological Macromolecules, 134*, 946–953. https://doi.org/10.1016/J.IJBIOMAC.2019.05.035

Akhavan, A., & Ataeevarjovi, E. (2012). The effect of gamma irradiation and surfactants on the size distribution of nanoparticles based on soluble starch. *Radiation Physics and Chemistry, 81*(7), 913–914. https://doi.org/10.1016/J.RADPHYSCHEM.2012.03.004

Andrade, I. H. P., Otoni, C. G., Amorim, T. S., Camilloto, G. P., & Cruz, R. S. (2020). Ultrasound-assisted extraction of starch nanoparticles from breadfruit (Artocarpus altilis (Parkinson) Fosberg). *Colloids and Surfaces A: Physicochemical and Engineering Aspects, 586*, Article 124277. https://doi.org/10.1016/J.COLSURFA.2019.124277

Angellier, H., Putaux, J. L., Molina-Boisseau, S., Dupeyre, D., & Dufresne, A. (2005). Starch nanocrystal fillers in an acrylic polymer matrix. *Macromolecular Symposia, 221*(1), 95–104. https://doi.org/10.1002/MASY.200550310

Apostolidis, E., Kioupis, D., Kakali, G., Stoforos, N. G., & Mandala, I. (2021). Effect of starch concentration and resistant starch filler addition on the physical properties of starch hydrogels. *Journal of Food Science, 86*(12), 5340–5352. https://doi.org/10.1111/1750-3841.15954

Apostolidis, E., & Mandala, I. (2020). Modification of resistant starch nanoparticles using high-pressure homogenization treatment. *Food Hydrocolloids, 103*, Article 105677. https://doi.org/10.1016/j.foodhyd.2020.105677

Aytunga, E., Kibar, A., Gönenç, İ., & Us, F. (2010). *Gelatinization of waxy, normal and high amylose corn starches*.

Azad, M. M., Ejaz, M., Shah, A. ur R., Afaq, S. K., & Song, J. (2022). A bio-based approach to simultaneously improve flame retardancy, thermal stability and mechanical properties of nano-silica filled jute/thermoplastic starch composite. *Materials Chemistry and Physics, 289*, Article 126485. https://doi.org/10.1016/J.MATCHEMPHYS.2022.126485

Babu, A. S., Mohan, R. J., & Parimalavalli, R. (2019). Effect of single and dual-modifications on stability and structural characteristics of foxtail millet starch. *Food Chemistry, 271*, 457–465. https://doi.org/10.1016/J.FOODCHEM.2018.07.197

Beaucage, G. (2004). Determination of branch fraction and minimum dimension of mass-fractal aggregates. *Physical Review E - Statistical Physics, Plasmas, Fluids, and Related Interdisciplinary Topics, 70*(3), 10. https://doi.org/10.1103/PHYSREVE.70.031401/FIGURES/6/MEDIUM

Beaucage, G., & Schaefer, D. W. (1994). Structural studies of complex systems using small-angle scattering: A unified guinier/power-law approach. *Journal of Non-crystalline Solids, 172–174*(2), 797–805. https://doi.org/10.1016/0022-3093(94)90581-9

Benmoussa, M., Moldenhauer, K. A. K., & Hamaker, B. R. (2007). Rice amylopectin fine structure variability affects starch digestion properties. *Journal of Agricultural and Food Chemistry, 55*(4), 1475–1479. https://doi.org/10.1021/JF062349X/ASSET/IMAGES/LARGE/JF062349XF00001.JPEG

Bertoft, E. (2017). Understanding starch structure: Recent progress. Page 56, 7 *Agronomy 2017, 7*(3), 56. https://doi.org/10.3390/AGRONOMY7030056.

Boufi, S., Bel Haaj, S., Magnin, A., Pignon, F., Impéror-Clerc, M., & Mortha, G. (2018). Ultrasonic assisted production of starch nanoparticles: Structural characterization and mechanism of disintegration. *Ultrasonics Sonochemistry, 41*, 327–336. https://doi.org/10.1016/J.ULTSONCH.2017.09.033

Brust, H., Orzechowski, S., & Fettke, J. (2020). Starch and glycogen analyses: Methods and techniques. Page 1020, 10 *Biomolecules 2020, 10*(7), 1020. https://doi.org/10.3390/BIOM10071020.

Bu, X., Wang, X., Dai, L., Ji, N., Xiong, L., & Sun, Q. (2020). The combination of starch nanoparticles and Tween 80 results in enhanced emulsion stability. *International Journal of Biological Macromolecules, 163*, 2048–2059. https://doi.org/10.1016/J.IJBIOMAC.2020.09.111

Carmona-García, R., Bello-Pérez, L. A., Aguirre-Cruz, A., Aparicio-Saguilán, A., Hernández-Torres, J., & Alvarez-Ramirez, J. (2016). Effect of ultrasonic treatment on the morphological, physicochemical, functional, and rheological properties of starches with different granule size. *Starch - Stärke, 68*(9–10), 972–979. https://doi.org/10.1002/STAR.201600019

Chang, Y., Yan, X., Wang, Q., Ren, L., Tong, J., & Zhou, J. (2017). High efficiency and low cost preparation of size controlled starch nanoparticles through ultrasonic treatment and precipitation. *Food Chemistry, 227*, 369–375. https://doi.org/10.1016/J.FOODCHEM.2017.01.111

Chao, D., Chen, J., Dong, Q., Wu, W., Qi, D., & Dong, S. (2020). Ultrastable and ultrasensitive pH-switchable carbon dots with high quantum yield for water quality identification, glucose detection, and two starch-based solid-state fluorescence materials, 13:11 *Nano Research 2020, 13*(11), 3012–3018. https://doi.org/10.1007/S12274-020-2965-8.

Chinnasamy, G., Dekeba, K., Sundramurthy, V. P., & Dereje, B. (2022), 10.1080/10942912.2022.2098973. In *Physicochemical properties of tef starch: Morphological, thermal, thermogravimetric, and pasting properties* (Vol. 25, pp. 1668–1682). https://doi.org/10.1080/10942912.2022.2098973, 1.

Chung, H. J., Liu, Q., Lee, L., & Wei, D. (2011). Relationship between the structure, physicochemical properties and in vitro digestibility of rice starches with different amylose contents. *Food Hydrocolloids, 25*(5), 968–975. https://doi.org/10.1016/J.FOODHYD.2010.09.011

Chutia, H., & Mahanta, C. L. (2021). Properties of starch nanoparticle obtained by ultrasonication and high pressure homogenization for developing carotenoids-enriched powder and Pickering nanoemulsion. *Innovative Food Science & Emerging Technologies, 74*, Article 102822. https://doi.org/10.1016/J.IFSET.2021.102822

Copeland, L., Blazek, J., Salman, H., & Tang, M. C. (2009). Form and functionality of starch. *Food Hydrocolloids, 23*(6), 1527–1534. https://doi.org/10.1016/J.FOODHYD.2008.09.016

Dai, L., Li, C., Zhang, J., & Cheng, F. (2018). Preparation and characterization of starch nanocrystals combining ball milling with acid hydrolysis. *Carbohydrate Polymers, 180*, 122–127. https://doi.org/10.1016/J.CARBPOL.2017.10.015

Dong, H., Zhang, Q., Gao, J., Chen, L., & Vasanthan, T. (2021). Comparison of morphology and rheology of starch nanoparticles prepared from pulse and cereal starches by rapid antisolvent nanoprecipitation. *Food Hydrocolloids, 119*, Article 106828. https://doi.org/10.1016/J.FOODHYD.2021.106828

Dong, H., Zhang, Q., Gao, J., Chen, L., & Vasanthan, T. (2022). Preparation and characterization of nanoparticles from cereal and pulse starches by ultrasonic-assisted dissolution and rapid nanoprecipitation. *Food Hydrocolloids, 122*, Article 107081. https://doi.org/10.1016/J.FOODHYD.2021.107081

Doutch, J., & Gilbert, E. P. (2013). Characterisation of large scale structures in starch granules via small-angle neutron and X-ray scattering. *Carbohydrate Polymers, 91*(1), 444–451. https://doi.org/10.1016/J.CARBPOL.2012.08.002

Dundar, A. N., & Gocmen, D. (2013). Effects of autoclaving temperature and storing time on resistant starch formation and its functional and physicochemical properties. *Carbohydrate Polymers, 97*(2), 764–771. https://doi.org/10.1016/J.CARBPOL.2013.04.083

Duyen, T. T. M., & Van Hung, P. (2021). Morphology, crystalline structure and digestibility of debranched starch nanoparticles varying in average degree of polymerization and fabrication methods. *Carbohydrate Polymers, 256*, Article 117424. https://doi.org/10.1016/J.CARBPOL.2020.117424

Englyst, H., Kingman, S. M., & Cummings, J. H. (1992). Classification and measurement of nutritionally important starch fractions. Suppl 2 *European Journal of Clinical Nutrition, 46*(2), S33–S50 https://europepmc.org/article/med/1330528.

Englyst, H., Wiggins, H. S., & Cummings, J. H. (1982). Determination of the non-starch polysaccharides in plant foods by gas-liquid chromatography of constituent sugars as alditol acetates. *Analyst, 107*(1272), 307–318. https://doi.org/10.1039/AN9820700307

Faille, C., Lemy, C., Allion-Maurer, A., & Zoueshtiagh, F. (2019). Evaluation of the hydrophobic properties of latex microspheres and Bacillus spores. Influence of the particle size on the data obtained by the MATH method (microbial adhesion to hydrocarbons). *Colloids and Surfaces B: Biointerfaces, 182*, Article 110398. https://doi.org/10.1016/J.COLSURFB.2019.110398

Falsafi, S. R., Maghsoudlou, Y., Rostamabadi, H., Rostamabadi, M. M., Hamedi, H., & Hosseini, S. M. H. (2019). Preparation of physically modified oat starch with different sonication treatments. *Food Hydrocolloids, 89*, 311–320. https://doi.org/10.1016/J.FOODHYD.2018.10.046

Fang, J. M., Fowler, P. A., Tomkinson, J., & Hill, C. A. S. (2002). The preparation and characterisation of a series of chemically modified potato starches. *Carbohydrate Polymers, 47*(3), 245–252. https://doi.org/10.1016/S0144-8617(01)00187-4

Fitzgerald, M. A., Rahman, S., Resurreccion, A. P., Concepcion, J., Daygon, V. D., Dipti, S. S., Kabir, K. A., Klingner, B., Morell, M. K., & Bird, A. R. (2011). Identification of a major genetic determinant of glycaemic index in rice. *Rice, 4*(2), 66–74. https://doi.org/10.1007/S12284-011-9073-Z/FIGURES/4

Guida, C., Aguiar, A. C., & Cunha, R. L. (2021). Green techniques for starch modification to stabilize pickering emulsions: A current review and future perspectives. *Current Opinion in Food Science, 38*, 52–61. https://doi.org/10.1016/J.COFS.2020.10.017

Hernandez-Hernandez, O., Julio-Gonzalez, L. C., Doyagüez, E. G., & Gutiérrez, T. J. (2022). Structure-digestibility relationship from noodles based on organocatalytically esterified regular and waxy corn starch obtained by reactive extrusion using sodium propionate. *Food Hydrocolloids, 131*, Article 107825. https://doi.org/10.1016/J.FOODHYD.2022.107825

Huang, Q., Huang, Q., Wang, Y., & Lu, X. (2022). Development of wet media milled purple sweet potato particle-stabilized pickering emulsions: The synergistic role of bioactives, starch and cellulose. *Lebensmittel-Wissenschaft & Technologie, 155*, Article 112964. https://doi.org/10.1016/J.LWT.2021.112964

Hu, A., Li, L., Zheng, J., Lu, J., Meng, X., & Liu, Y. (2014). Different-frequency ultrasonic effects on properties and structure of corn starch. *Journal of the Science of Food and Agriculture, 94*(14), 2929–2934. https://doi.org/10.1002/JSFA.6636

Jenkins, P. J., & Donald, A. M. (1998). Gelatinisation of starch: A combined SAXS/WAXS/DSC and SANS study. *Carbohydrate Research, 308*(1–2), 133–147. https://doi.org/10.1016/S0008-6215(98)00079-2

Jeong, O., & Shin, M. (2018). Preparation and stability of resistant starch nanoparticles, using acid hydrolysis and cross-linking of waxy rice starch. *Food Chemistry, 256*, 77–84. https://doi.org/10.1016/J.FOODCHEM.2018.02.098

Jiang, S., Dai, L., Qin, Y., Xiong, L., & Sun, Q. (2016). Preparation and characterization of octenyl succinic anhydride modified taro starch nanoparticles. *PLoS One, 11*(2), Article e0150043. https://doi.org/10.1371/JOURNAL.PONE.0150043

Jiang, F., Du, C., Zhao, N., Jiang, W., Yu, X., & Du, S. kui (2022). Preparation and characterization of quinoa starch nanoparticles as quercetin carriers. *Food Chemistry, 369*, Article 130895. https://doi.org/10.1016/J.FOODCHEM.2021.130895

Junejo, S. A., Flanagan, B. M., Zhang, B., & Dhital, S. (2022). Starch structure and nutritional functionality – past revelations and future prospects. *Carbohydrate Polymers, 277*, Article 118837. https://doi.org/10.1016/J.CARBPOL.2021.118837

Kaczmarska, K., Grabowska, B., Spychaj, T., Zdanowicz, M., Sitarz, M., Bobrowski, A., & Cukrowicz, S. (2018). Effect of microwave treatment on structure of binders based on sodium carboxymethyl starch: FT-IR, FT-Raman and XRD investigations. *Spectrochimica Acta Part A: Molecular and Biomolecular Spectroscopy, 199*, 387–393. https://doi.org/10.1016/J.SAA.2018.03.047

Kizil, R., Irudayaraj, J., & Seetharaman, K. (2002). Characterization of irradiated starches by using FT-Raman and FTIR spectroscopy. *Journal of Agricultural and Food Chemistry, 50*(14), 3912–3918. https://doi.org/10.1021/JF011652P

Ko, E. B., & Kim, J. Y. (2021). Application of starch nanoparticles as a stabilizer for Pickering emulsions: Effect of environmental factors and approach for enhancing its storage stability. *Food Hydrocolloids, 120*, Article 106984. https://doi.org/10.1016/J.FOODHYD.2021.106984

Kumar Malik, M., Kumar, T., Kumar, V., Singh, J., Kumar Singh, R., & Saini, K. (2022). Sustainable, highly foldable, eco-friendly films from Mandua starch derivative. *Sustainable Energy Technologies and Assessments, 53*, Article 102398. https://doi.org/10.1016/J.SETA.2022.102398

Lawal, M. V. (2019). Modified starches as direct compression excipients – effect of physical and chemical modifications on tablet properties: A review. *Starch - Stärke, 71*(1–2), Article 1800040. https://doi.org/10.1002/STAR.201800040

Lin, Q., Liu, Y., Zhou, L., Ji, N., Xiong, L., & Sun, Q. (2022). Green preparation of debranched starch nanoparticles with different crystalline structures by electrostatic spraying. *Food Hydrocolloids, 127*, Article 107513. https://doi.org/10.1016/J.FOODHYD.2022.107513

Liu, D., Wu, Q., Chen, H., & Chang, P. R. (2009). Transitional properties of starch colloid with particle size reduction from micro- to nanometer. *Journal of Colloid and Interface Science, 339*(1), 117–124. https://doi.org/10.1016/J.JCIS.2009.07.035

Liu, X., Zheng, J., Yang, Y., Chen, Y., & Liu, X. (2018). Preparation of N-doped carbon dots based on starch and their application in white LED. *Optical Materials, 86*, 530–536. https://doi.org/10.1016/J.OPTMAT.2018.10.057

Li, J. Y., & Yeh, A. I. (2001). Relationships between thermal, rheological characteristics and swelling power for various starches. *Journal of Food Engineering, 50*(3), 141–148. https://doi.org/10.1016/S0260-8774(00)00236-3

Li, Y., Zhao, L., Shi, L., Lin, L., Cao, Q., & Wei, C. (2022). Sizes, components, crystalline structure, and thermal properties of starches from sweet potato varieties originating from different countries, 27, Page 1905 *Molecules 2022, 27*(6), 1905. https://doi.org/10.3390/MOLECULES27061905.

Luo, X., Cheng, B., Zhang, W., Shu, Z., Wang, P., & Zeng, X. (2021). Structural and functional characteristics of Japonica rice starches with different amylose contents. *CyTA - Journal of Food, 19*(1), 532–540. https://doi.org/10.1080/19476337.2021.1927194. http://Mc.Manuscriptcentral.Com/Tcyt

Mandala, I. G., & Bayas, E. (2004). Xanthan effect on swelling, solubility and viscosity of wheat starch dispersions. *Food Hydrocolloids, 18*(2), 191–201. https://doi.org/10.1016/S0268-005X(03)00064-X

Maniglia, B. C., Castanha, N., Le-Bail, P., Le-Bail, A., & Augusto, P. E. D. (2020). Https://Doi.Org/10.1080/10408398.2020.1778633. In *Starch modification through environmentally friendly alternatives: A review* (Vol. 61, pp. 2482–2505). https://doi.org/10.1080/10408398.2020.1778633, 15.

Maurya, A. K., Weidenbacher, L., Spano, F., Fortunato, G., Rossi, R. M., Frenz, M., Dommann, A., Neels, A., & Sadeghpour, A. (2019). Structural insights into semicrystalline states of electrospun nanofibers: A multiscale analytical approach. *Nanoscale, 11*(15), 7176–7187. https://doi.org/10.1039/C9NR00446G

Ma, X., Yu, J., He, K., & Wang, N. (2007). The effects of different plasticizers on the properties of thermoplastic starch as solid polymer electrolytes. *Macromolecular Materials and Engineering, 292*(4), 503–510. https://doi.org/10.1002/MAME.200600445

Monroy, Y., Rivero, S., & García, M. A. (2018). Microstructural and techno-functional properties of cassava starch modified by ultrasound. *Ultrasonics Sonochemistry, 42*, 795–804. https://doi.org/10.1016/J.ULTSONCH.2017.12.048

Nain, V., Kaur, M., Sandhu, K. S., Thory, R., & Sinhmar, A. (2022). Development of starch nanoparticle from mango kernel in comparison with cereal, tuber, and legume starch nanoparticles: Characterization and cytotoxicity. *Starch - Stärke, 74*(3–4), Article 2100252. https://doi.org/10.1002/STAR.202100252

Navaf, M., Sunooj, K. V., Aaliya, B., Sudheesh, C., & George, J. (2020). Physico-chemical, functional, morphological, thermal properties and digestibility of Talipot palm (Corypha umbraculifera L.) flour and starch grown in Malabar region of South India. *Journal of Food Measurement and Characterization, 14*(3), 1601–1613. https://doi.org/10.1007/S11694-020-00408-1

Noor, N., Gani, A., Jhan, F., Ashraf Shah, M., & ul Ashraf, Z. (2022). Ferulic acid loaded pickering emulsions stabilized by resistant starch nanoparticles using ultrasonication: Characterization, in vitro release and nutraceutical potential. *Ultrasonics Sonochemistry, 84*, Article 105967. https://doi.org/10.1016/J.ULTSONCH.2022.105967

Noor, N., Gani, A., Jhan, F., Jenno, J. L. H., & Arif Dar, M. (2021). Resistant starch type 2 from lotus stem: Ultrasonic effect on physical and nutraceutical properties. *Ultrasonics Sonochemistry, 76*, Article 105655. https://doi.org/10.1016/J.ULTSONCH.2021.105655

Pérez, S., & Bertoft, E. (2010). The molecular structures of starch components and their contribution to the architecture of starch granules: A comprehensive review. *Starch - Stärke, 62*(8), 389–420. https://doi.org/10.1002/STAR.201000013

Pinotsi, D., Grisanti, L., Mahou, P., Gebauer, R., Kaminski, C. F., Hassanali, A., & Kaminski Schierle, G. S. (2016). Proton transfer and structure-specific fluorescence in hydrogen bond-rich protein structures. *Journal of the American Chemical Society, 138*(9), 3046–3057. https://doi.org/10.1021/JACS.5B11012/SUPPL_FILE/JA5B11012_SI_004.AVI

Qin, Y., Liu, C., Jiang, S., Xiong, L., & Sun, Q. (2016). Characterization of starch nanoparticles prepared by nanoprecipitation: Influence of amylose content and starch type. *Industrial Crops and Products, 87*, 182–190. https://doi.org/10.1016/J.INDCROP.2016.04.038

Qiu, C., Hu, Y., Jin, Z., McClements, D. J., Qin, Y., Xu, X., & Wang, J. (2019). A review of green techniques for the synthesis of size-controlled starch-based nanoparticles and their applications as nanodelivery systems. *Trends in Food Science & Technology, 92*, 138–151. https://doi.org/10.1016/J.TIFS.2019.08.007

Qiu, C., Yang, J., Ge, S., Chang, R., Xiong, L., & Sun, Q. (2016). Preparation and characterization of size-controlled starch nanoparticles based on short linear chains from debranched waxy corn starch. *Lebensmittel-Wissenschaft & Technologie, 74*, 303–310. https://doi.org/10.1016/J.LWT.2016.07.062

Rahaman, A., Kumari, A., Zeng, X. A., Adil Farooq, M., Siddique, R., Khalifa, I., Siddeeg, A., Ali, M., & Faisal Manzoor, M. (2021). Ultrasound based modification and structural-functional analysis of corn and cassava starch. *Ultrasonics Sonochemistry, 80*, Article 105795. https://doi.org/10.1016/J.ULTSONCH.2021.105795

Ren, Y., Yuan, T. Z., Chigwedere, C. M., & Ai, Y. (2021). A current review of structure, functional properties, and industrial applications of pulse starches for value-added utilization. *Comprehensive Reviews in Food Science and Food Safety, 20*(3), 3061–3092. https://doi.org/10.1111/1541-4337.12735

Ruan, S., Tang, J., Qin, Y., Wang, J., Yan, T., Zhou, J., Gao, D., Xu, E., & Liu, D. (2022). Mechanical force-induced dispersion of starch nanoparticles and nanoemulsion: Size control, dispersion behaviour, and emulsified stability. *Carbohydrate Polymers, 275*, Article 118711. https://doi.org/10.1016/J.CARBPOL.2021.118711

Saari, H., Fuentes, C., Sjöö, M., Rayner, M., & Wahlgren, M. (2017). Production of starch nanoparticles by dissolution and non-solvent precipitation for use in food-grade Pickering emulsions. *Carbohydrate Polymers, 157*, 558–566. https://doi.org/10.1016/J.CARBPOL.2016.10.003

Sanver, D., Sadeghpour, A., Rappolt, M., Di Meo, F., & Trouillas, P. (2020). Structure and dynamics of dioleoyl-phosphatidylcholine Bilayers under the influence of quercetin and rutin. *Langmuir, 36*(40), 11776–11786. https://doi.org/10.1021/ACS.LANGMUIR.0C01484/SUPPL_FILE/LA0C01484_SI_002.ZIP

Shahbazi, M., Majzoobi, M., & Farahnaky, A. (2018). Physical modification of starch by high-pressure homogenization for improving functional properties of κ-carrageenan/starch blend film. *Food Hydrocolloids, 85*, 204–214. https://doi.org/10.1016/J.FOODHYD.2018.07.017

Shibata, H., Abe, M., Sato, K., Uwai, K., Tokuraku, K., & Iimori, T. (2022). Microwave-assisted synthesis and formation mechanism of fluorescent carbon dots from starch. *Carbohydrate Polymer Technologies and Applications, 3*, Article 100218. https://doi.org/10.1016/J.CARPTA.2022.100218

Sun, Q., Li, G., Dai, L., Ji, N., & Xiong, L. (2014). Green preparation and characterisation of waxy maize starch nanoparticles through enzymolysis and recrystallisation. *Food Chemistry, 162*, 223–228. https://doi.org/10.1016/J.FOODCHEM.2014.04.068

Sun, M., Qu, S., Hao, Z., Ji, W., Jing, P., Zhang, H., Zhang, L., Zhao, J., & Shen, D. (2014). Towards efficient solid-state photoluminescence based on carbon-nanodots and starch composites. *Nanoscale, 6*(21), 13076–13081. https://doi.org/10.1039/C4NR04034A

Timgren, A., Rayner, M., Dejmek, P., Marku, D., Sj, M., & Marilyn Rayner, C. (2013). Emulsion stabilizing capacity of intact starch granules modified by heat treatment or octenyl succinic anhydride. *Food Sciences and Nutrition, 1*(2), 157–171. https://doi.org/10.1002/FSN3.17

Torres, F. G., & De-la-Torre, G. E. (2022). Synthesis, characteristics, and applications of modified starch nanoparticles: A review. *International Journal of Biological Macromolecules, 194*, 289–305. https://doi.org/10.1016/J.IJBIOMAC.2021.11.187

Troncoso, O. P., & Torres, F. G. (2020). Bacterial cellulose—graphene based nanocomposites, 21, Page 6532 *International Journal of Molecular Sciences 2020, 21*(18), 6532. https://doi.org/10.3390/IJMS21186532.

Ullah, I., Yin, T., Xiong, S., Huang, Q., Zia-ud-Din, Zhang, J., & Javaid, A. B. (2018). Effects of thermal pre-treatment on physicochemical properties of nano-sized okara (soybean residue) insoluble dietary fiber prepared by wet media milling. *Journal of Food Engineering, 237*, 18–26. https://doi.org/10.1016/J.JFOODENG.2018.05.017

Vamadevan, V., & Bertoft, E. (2015). Structure-function relationships of starch components. *Starch - Stärke, 67*(1–2), 55–68. https://doi.org/10.1002/STAR.201400188

Wang, H., Xu, K., Ma, Y., Liang, Y., Zhang, H., & Chen, L. (2020). Impact of ultrasonication on the aggregation structure and physicochemical characteristics of sweet potato starch. *Ultrasonics Sonochemistry, 63*, Article 104868. https://doi.org/10.1016/J.ULTSONCH.2019.104868

Wang, R., & Zhou, J. (2022). Waxy maize starch nanoparticles incorporated tea polyphenols to stabilize Pickering emulsion and inhibit oil oxidation. *Carbohydrate Polymers, 296*, Article 119991. https://doi.org/10.1016/J.CARBPOL.2022.119991

Warren, F. J., Gidley, M. J., & Flanagan, B. M. (2016). Infrared spectroscopy as a tool to characterise starch ordered structure—a joint FTIR–ATR, NMR, XRD and DSC study. *Carbohydrate Polymers, 139*, 35–42. https://doi.org/10.1016/J.CARBPOL.2015.11.066

Wei, B., Hu, X., Li, H., Wu, C., Xu, X., Jin, Z., & Tian, Y. (2014). Effect of pHs on dispersity of maize starch nanocrystals in aqueous medium. *Food Hydrocolloids, 36*, 369–373. https://doi.org/10.1016/J.FOODHYD.2013.08.015

Xing, J. jie, Liu, Y., Li, D., Wang, L. jun, & Adhikari, B. (2017). Heat-moisture treatment and acid hydrolysis of corn starch in different sequences. *LWT - Food Science and Technology, 79*, 11–20. https://doi.org/10.1016/J.LWT.2016.12.055

Yang, Q., Liu, L., Li, X., Li, J., Zhang, W., Shi, M., & Feng, B. (2021). Http://Mc.Manuscriptcentral.Com/Tcyt. In *Physicochemical characteristics of resistant starch prepared from Job's tears starch using autoclaving–cooling treatment* (Vol. 19, pp. 316–325). https://doi.org/10.1080/19476337.2021.1897688, 1.

Yang, Q. Y., Lu, X. X., Chen, Y. Z., Luo, Z. G., & Xiao, Z. G. (2019). Fine structure, crystalline and physicochemical properties of waxy corn starch treated by ultrasound irradiation. *Ultrasonics Sonochemistry, 51*, 350–358. https://doi.org/10.1016/J.ULTSONCH.2018.09.001

Yan, Z., Shu, J., Yu, Y., Zhang, Z., Liu, Z., & Chen, J. (2015). Preparation of carbon quantum dots based on starch and their spectral properties. *Luminescence, 30*(4), 388–392. https://doi.org/10.1002/BIO.2744

Zhang, M., Xu, Z., & Wang, L. (2022). Ultrasonic treatment improves the performance of starch as depressant for hematite flotation. *Ultrasonics Sonochemistry, 82*, Article 105877. https://doi.org/10.1016/J.ULTSONCH.2021.105877

Zhao, T., Zhang, H., Chen, F., Tong, P., Cao, W., & Jiang, Y. (2022). *Study on structural changes of starches with different amylose content during gelatinization process*. Starch - Stärke. https://doi.org/10.1002/STAR.202100269, 2100269.

Zhong, Y., Bertoft, E., Li, Z., Blennow, A., & Liu, X. (2020). Amylopectin starch granule lamellar structure as deduced from unit chain length data. *Food Hydrocolloids, 108*, Article 106053. https://doi.org/10.1016/J.FOODHYD.2020.106053

Zhou, D., Ma, Z., Yin, X., Hu, X., & Boye, J. I. (2019). Structural characteristics and physicochemical properties of field pea starch modified by physical, enzymatic, and acid treatments. *Food Hydrocolloids, 93*, 386–394. https://doi.org/10.1016/J.FOODHYD.2019.02.048

Zhu, T., Jackson, D. S., Wehling, R. L., & Geera, B. (2008). Comparison of amylose determination methods and the development of a dual wavelength iodine binding technique. *Cereal Chemistry, 85*(1), 51–58. https://doi.org/10.1094/CCHEM-85-1-0051

Zhu, J., Li, L., Chen, L., & Li, X. (2012). Study on supramolecular structural changes of ultrasonic treated potato starch granules. *Food Hydrocolloids, 29*(1), 116–122. https://doi.org/10.1016/J.FOODHYD.2012.02.004

Zhu, L. J., Liu, Q. Q., Wilson, J. D., Gu, M. H., & Shi, Y. C. (2011). Digestibility and physicochemical properties of rice (Oryza sativa L.) flours and starches differing in amylose content. *Carbohydrate Polymers, 86*(4), 1751–1759. https://doi.org/10.1016/J.CARBPOL.2011.07.017